Ferroelastic dynamics and strain compatibility

T. Lookman,[1] S. R. Shenoy,[2] K. Ø. Rasmussen,[1] A. Saxena,[1] and A. R. Bishop[1]
[1]*Theoretical Division and Center for Nonlinear Studies, Los Alamos National Laboratory, Los Alamos, New Mexico 87545*
[2]*Abdus Salam International Centre for Theoretical Physics, 34100 Trieste, Italy*
(Received 10 April 2002; revised manuscript received 8 August 2002; published 31 January 2003)

We derive underdamped evolution equations for the order-parameter (OP) strains of a proper ferroelastic material undergoing a structural transition, using Lagrangian variations with Rayleigh dissipation, and a free energy as a polynomial expansion in the $N=n+N_{op}$ symmetry-adapted strains. The N_{op} strain equations are structurally similar in form to the Lagrange-Rayleigh one-dimensional strain dynamics of Bales and Gooding (BG), with ''strain accelerations'' proportional to a Laplacian acting on a sum of the free-energy strain derivative and frictional strain force assuming geometric linearity. The tensorial St. Venant's elastic compatibility constraints that forbid defects, are used to determine the n non-order-parameter strains in terms of the OP strains, generating anisotropic and long-range OP contributions to the free energy, friction, and noise. The *same* OP equations are obtained by either varying the displacement vector components, or by varying the N strains subject to the N_c compatibility constraints. A Fokker-Planck equation, based on the BG dynamics in more than one dimension with noise terms, is set up. The BG dynamics corresponds to a set of nonidentical nonlinear (strain) oscillators labeled by wave vector $\vec{k}$, with competing short- and long-range couplings. The oscillators have different ''strain-mass'' densities $\rho(k)\sim 1/k^2$ and dampings $\sim 1/\rho(k)\sim k^2$, so the lighter large-k oscillators equilibrate first, corresponding to earlier formation of smaller-scale oriented textures. This produces a sequential-scale scenario for post-quench nucleation, elastic patterning, and hierarchical growth. Neglecting inertial effects yields a late-time dynamics for identifying extremal free-energy states, that is, of the time-dependent Ginzburg-Landau form, with nonlocal, anisotropic Onsager coefficients that become constants for special parameter values. We consider in detail the two-dimensional (2D) unit-cell transitions from a triangular to a centered rectangular lattice ($N_{op}=2,n=1,N_c=1$) and from a square to a rectangular lattice ($N_{op}=1,n=2,N_c=1$) for which the OP compatibility kernel is retarded in time, or frequency dependent in Fourier space (in fact, acoustically resonant in ω/k). We present structural dynamics for all other 2D symmetry-allowed proper ferroelastic transitions: the procedure is also applicable to the 3D case. Simulations of the BG evolution equations confirm the inherent richness of the static and dynamic texturings, including strain oscillations, domain-wall propagation at near-sound speeds, grain-boundary motion, and nonlocal ''elastic photocopying'' of imposed local stress patterns.

DOI: 10.1103/PhysRevB.67.024114 PACS number(s): 64.70.Kb, 64.60.Cn, 11.10.Lm, 81.30.Kf

I. INTRODUCTION

Structural phase transitions in solids have attracted a great deal of interest over a century, both for their conceptual importance as symmetry-changing phase transitions, and for their role in inducing technologically useful properties in materials. Both the diffusion-controlled replacive and the diffusionless displacive transformations have been studied, although the former have received more attention because their reaction kinetics is more conducive to control.

We consider here the class of materials known as ferroelastic martensites. Ferroelasticity is defined as the existence of two or more stable orientation states of a crystal that correspond to different arrangements of the atoms, but are structurally identical or enantiomorphous.[1,2] In addition, these orientation states are degenerate in energy in the absence of mechanical stress. The term ''martensitic'' refers to a diffusionless first-order phase transition that can be described in terms of one (or several successive) shear deformation(s) from a parent to a product phase.[3] The morphology and kinetics of the transition are dominated by the strain energy. The transition results in a characteristic lamellar or twinned microstructure.

Salient features of proper ferroelastic crystals include mechanical hysteresis and mechanically (reversibly) switchable domain patterns. Usually ferroelasticity occurs as a result of a phase transition from a nonferroelastic high-symmetry ''parent'' phase and is associated with the softening of an elastic modulus with decreasing temperature or increasing pressure in the parent phase. Since the ferroelastic transition is normally weakly first order, or second order, it can be described to a good approximation by the Landau theory with spontaneous strain or deviation of a given ferroelastic orientation state from the parent phase as the order parameter. The strain can be coupled to other fields such as electric polarization and magnetic moment and thus the crystal can have more than one transition. Depending on whether the spontaneous strain is the primary or a secondary order parameter at a given transition, the lower symmetry phase is called a proper or an improper ferroelastic, respectively. While some martensites are proper ferroelastics, examples of improper ferroelastics include ferroelectrics and magnetoelastics.

There is a further subset of ferroelastic martensites (either nonelemental metals or alloy systems) that exhibit the shape memory effect.[4] These materials are characterized by highly mobile twin boundaries and (often) show precursor structures above the transition. Furthermore, these materials have

small Bain strain, elastic shear modulus softening, and a weakly to moderately first-order transition. Some examples include InTl, FePd, NiTi, and AuCd.

Dynamics plays a central role in proper ferroelastic transitions.[2,5–17] As noted, these materials undergo diffusionless, displacive transitions, with strain (components) as the primary order parameter, and develop complex microstructures in their dynamical evolution, finally forming spatially varying, multiscale ''textures'' or strain patterns. When quenched, some martensitic materials develop interfaces moving at near-sound speeds. Textured improper ferroelastics include materials of technological importance such as superconducting cuprates[18] and colossal magnetoresistance manganites.[19] Many dynamical models have been invoked to follow aspects of (proper) ferroelastic pattern formation[5–17] such as nucleated twin-front propagation, width-length scaling of twin dimensions,[20,21] tweed,[22–24] stress effects, elastic domain misfits, and acoustic noise generation.[25]

In a one-dimensional (1D) model, Bales and Gooding[5] considered a displacement u and a sixth-order free energy $F(\varepsilon)$, nonlinear in the strain, that in one dimension is simply a derivative, $\varepsilon = \partial u/\partial x$. With Lagrangian dynamics, a Rayleigh dissipation,[26] and variation in u, a single strain evolution equation was obtained in one dimension,

$$\rho_0 \ddot{\varepsilon} = \frac{\partial^2}{\partial x^2}\left(\frac{\delta F}{\delta \varepsilon} + A' \dot{\varepsilon}\right), \tag{1.1}$$

where A' and ρ_0 are the scaled friction (coefficient) and mass density, respectively. In a low-frequency–large-wave-vector regime $\rho_0 \omega \ll A' k^2$, where the inertial term is small, a simple time-dependent Ginzburg-Landau (TDGL) equation is obtained[5,6] in one dimension,

$$\dot{\varepsilon} = -\frac{1}{A'}\frac{\delta F}{\delta \varepsilon}. \tag{1.2}$$

For the $k \neq 0$ modes in one dimension the strain is a one-component ''vector'' that in Fourier space is simply proportional to the scalar displacement; and there is only one Bravais lattice. In higher dimensions $D>1$, the strain (displacement) is a tensor (vector), and there are many possible discrete lattice symmetries. The central question is: what is the general form of the underdamped evolution equations for (order-parameter) strain-tensor components, for ferroelastic transitions of different symmetries?

A wide variety of dynamical models have been used to date. These include a 2D or 3D TDGL dynamics in morphological variables for structural variants, with a long-range potential between squares of these variables,[8] motivated by ideas of elastic inclusions.[27] Other work in 2D and 3D has used a TDGL equation for the order-parameter (OP) strains only, with a long-range potential emerging between the OP strains themselves[10–12] (not their squares), by optimizing non-OP strains. Some authors[14] assumed the validity of a 2D Bales-Gooding (BG) form from a Lagrangian without non-OP strains, and then phenomenologically added a long-range potential between squares of the OP strains. A TDGL equation in the displacements has also been used.[13] Yet other models considered displacement accelerations equated to displacement gradients of the free energy as forces; or strain TDGL equations coupled to vacancy field dynamics.[15] Finally, the Lagrange-Rayleigh procedure[5,6,26] has recently been applied[16,17] in two dimensions, yielding an underdamped dynamics for the displacement, which is truncated to overdamped equations that are seemingly different from the TDGL form.

While these and other models yield valuable insights into ferroelastic texturing (i.e., single-crystal microstructure), there is clearly a need, through explicit derivation, to obtain an underdamped, symmetry-specific OP strain dynamics for $D>1$; to find the precise form of long-range potentials (if any) that emerge; and to determine the regime of validity (if it exists) of some form of TDGL equations.

In this paper, we use the Lagrange-Rayleigh variational procedure to derive a ferroelastic strain dynamics (including noise terms). A central role is played by the N_c St. Venant compatibility conditions[10,11,24,28–30] for the $N = N_{op} + n$ symmetry adapted strains, which enforce the absence of defects (and lattice integrity) at each instant, and allow the n non-OP strains to be expressed in terms of N_{op} order parameter strains. We show the following.

(i) An underdamped set of N_{op} equations can be obtained for the OP strains alone, which is of a generalized BG form, with naturally emerging anisotropic long-range (ALR) contributions to OP potentials, friction, and noise. (For the $N_{op} = 1$ case these are, in general, also explicitly *retarded* in time.)

(ii) The *same* OP equations can be obtained, either by varying the *displacement*, or by varying the *strains* subject to the compatibility constraint through dynamic Lagrange multipliers.

(iii) Dropping strain inertial terms yields strain TDGL equations, with nonlocal Onsager coefficients, that reduce to constants for special friction values, resulting in a local TDGL dynamics. These act as a late-time dynamics for the damping envelope of textural oscillations.

We explicitly demonstrate (i), (ii), (iii) above for the 2D triangular to centered rectangular or TR lattice transition ($N_{op}=2, n=1, N_c=1$) and for the square to rectangular or SR lattice transition ($N_{op}=1, n=2, N_c=1$), as well as present dynamics for all other allowed 2D symmetries. The procedure can be generalized to three dimensions, e.g., the cubic to tetragonal ($N_{op}=2, n=4, N_c=6$) transition where (static) compatibility potentials in a TDGL dynamics produce rich textures.[11] Our central result is a generalized BG dynamics written in the OP strains $\{\varepsilon_\ell\}$, $\ell = 1,2,\ldots,N_{op}$ only,

$$\rho_0 \ddot{\varepsilon}_\ell = \frac{c_\ell^2}{4}\vec{\Delta}^2\left(\frac{\delta(F+F^c)}{\delta \varepsilon_\ell} + \frac{\delta(R+R^c)}{\delta \dot{\varepsilon}_\ell}\right) + \tilde{g}_\ell + \tilde{g}_\ell^c, \tag{1.3}$$

where c_ℓ is a symmetry-specific constant, and ρ_0 is a scaled mass density. $F^c(\{\varepsilon_\ell\}), R^c(\{\dot{\varepsilon}_\ell\})$ are the compatibility-induced symmetry-specific contributions that emerge naturally from the non-OP free energy as additions to the OP free energy F and OP Rayleigh dissipation R, while $\tilde{g}_\ell^c$ is the

corresponding noise term that adds to the OP noise $\tilde{g}_\ell$. In Eq. (1.3) and subsequently, we use the symbol $\vec{\Delta}$ to denote dimensionless *discrete* derivatives on a reference lattice.[31] The generalized BG equations can be written as Langevin equation for $\varepsilon_\ell(\vec{k},t)$ and $v_\ell \equiv \dot{\varepsilon}_\ell(\vec{k},t)$, yielding statistically equivalent Fokker-Planck equations for the probability $P(\{\varepsilon_\ell, v_\ell\},t)$.

In the strain-variation derivation of the BG dynamics above, we introduce the concept of a strain mass-density tensor whose components (in Fourier space) behave as $\rho_{ss'}(k) \sim \rho_0/k^2$, which is responsible in coordinate space, for the Laplacian on the right-hand side of Eq. (1.3). This generalization of the 1D case expresses the physical idea that long-wavelength strains are extended lattice deformations and hence have greater inertia. We present a physically illuminating analogy of (generalized) BG dynamics as an array of coupled nonlinear $\vec{k}$-space oscillators that have an intrinsically hierarchical equilibration, with large k oscillators damping out first.

The N_{op} strain order-parameter equations with derived anisotropic long-range terms are equivalent to the D displacement equations that do not explicitly have such terms. The advantage of the OP strain approach is that it displays and uses such anisotropic long-range correlations that are valuable in understanding simulated textures, as demonstrated below.

More generally, in the displacement ($\vec{u}$) picture, the strains are derived quantities and the compatibility condition is an incidental identity, expressing the single-valuedness of $\vec{u}$. This is analogous to describing magnetic problems in terms of the vector potential $\vec{A}$, with $\vec{B}$ just a label for $\vec{\Delta} \times \vec{A}$, and with $\vec{\Delta} \cdot (\vec{\Delta} \times \vec{A}) = 0$ just expressing a vector identity. By contrast, in the strain-only picture, the geometrically linear strain tensor components $E_{\mu\nu}$ are the physical variables, and the compatibility conditions $\vec{\Delta} \times (\vec{\Delta} \times E)^T = 0$ (with T denoting transpose) are treated as independent field equations expressing the physical constraint of no defects. This is analogous to working with the magnetic induction $\vec{B}$, where the Maxwell's field equation $\vec{\Delta} \cdot \vec{B} = 0$ expresses the absence of magnetic monopoles. Similarly, the compatibility conditions can be viewed as the integrability conditions for the strain tensor as a function of (or with respect to) the displacement field.[30] The compatibility equation for strain has been used for a consistent description of forces in liquids;[30] here we use it to develop a consistent OP dynamics for ferroelastics.

The basic idea is quite simple. Compatibility implies non-OP strains $\{e_i\}$ are proportional in Fourier space to OP strains $\{\varepsilon_\ell\}$,

$$e_i = \sum_\ell S_{i\ell} \varepsilon_\ell . \tag{1.4}$$

It is convenient to henceforth notationally distinguish between n non-order-parameter strains $\{e_i\}$ and N_{op} order-parameter strains $\{\varepsilon_\ell\}$. The non-OP free energy f (and Rayleigh dissipation), harmonic in the non-OP strains (and time derivatives), can be written in terms of OP strains. With elastic constants a_i,

$$f = \frac{1}{2} \sum_{i,\vec{k}} a_i |e_i|^2 = \frac{1}{2} \sum_{\ell,\ell',\vec{k}} U_{\ell\ell'} \varepsilon_\ell \varepsilon^*_{\ell'} \equiv F^c(\{\varepsilon_\ell\}). \tag{1.5a}$$

This defines the compatibility kernels

$$U_{\ell\ell'} = \sum_i a_i S_{i\ell} S^*_{i\ell'} \tag{1.5b}$$

for F^c (and similarly for R^c) of Eq. (1.3) in the desired OP-only dynamics. Thus the problem reduces to finding the proportionality constants $S_{i\ell}$, for each symmetry-based phase transition.

The plan of the paper, with self-contained sections, is as follows. In Sec. II the OP dynamics for the TR case is derived by $\vec{u}$ variation. In Sec. III we demonstrate that the same TR dynamics is obtained by strain variation, with enforced compatibility. Results for the SR case are stated and analyzed, with derivation details in Appendix A. Numerical simulations of some interesting BG dynamic evolutions are presented (using standardized scaled energies[32] and dissipations, as in Appendix B). Noise contributions are derived, and a Fokker-Planck formalism is set up. Section IV discusses the equivalent inhomogeneous oscillator description of the BG dynamics. Section V deals with its TDGL truncation, also derived in Appendix C from truncated displacement dynamics.[16,17] Section VI presents the compatibility kernels for other 2D symmetries. Finally, Sec. VII contains a summary and discussion.

II. ORDER-PARAMETER STRAIN DYNAMICS BY DISPLACEMENT VARIATION

Consider a Lagrangian density $L(\alpha,\dot{\alpha}) = \int dt \Sigma_{\vec{r}} (T - V)$ that depends on a variable $\alpha(\vec{r},t)$ through a kinetic term $T = T(\dot{\alpha}) = \Sigma_{\vec{r}} \frac{1}{2} \rho_0 \dot{\alpha}^2$, and a potential term $V = V(\alpha)$. Then, with a Rayleigh dissipation[26] $R^{tot} \equiv R + R^c = \int d\vec{r} \frac{1}{2} \eta \dot{\alpha}^2$ (where η is the friction coefficient), we have, by variation in α, the Lagrange-Rayleigh equation,

$$\frac{d}{dt} \frac{\partial L}{\partial \dot{\alpha}} - \frac{\partial L}{\partial \alpha} = - \frac{\partial R^{tot}}{\partial \dot{\alpha}} . \tag{2.1}$$

In this section we work in the displacement picture, and consider variations in displacement $\alpha(\vec{r},t) \to u_\mu(\vec{r},t)$ that will generate $\mu = 1, \ldots, D$ equations, for $\ddot{u}_\mu$ in D dimensions. The potential or Gibbs free energy V depends on displacement derivatives that are $N = N_{op} + n$ symmetry-adapted linear combinations of the symmetric Cauchy strain tensor,

$$E_{\mu\nu} = \frac{1}{2} (\Delta_\mu u_\nu + \Delta_\nu u_\mu). \tag{2.2}$$

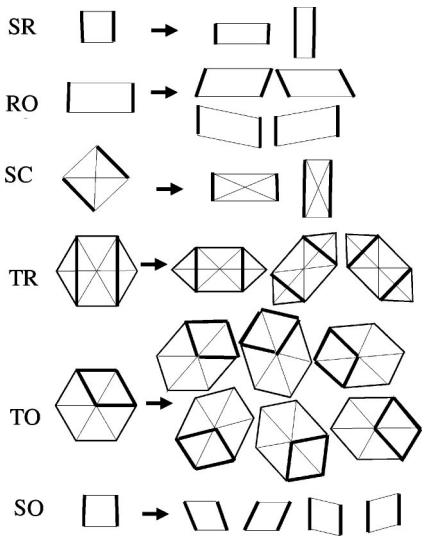

FIG. 1. Symmetry-allowed transitions in two-dimensions for the four crystal systems. The dark lines are guides to the eye, for deformations. There is a one-component strain order parameter for (a) the square to rectangle or SR case, driven by ε_2; (b) the rectangle to oblique or RO case, driven by ε_2; and (c) the square to centered rectangle or SC case, driven by ε_3. A two-component OP, or *two* one-component OP's, lead(s) to (d) the triangular to centered rectangle or TR case, driven by $\varepsilon_2, \varepsilon_3$; (e) the triangle to oblique or TO case, driven by $\varepsilon_2, \varepsilon_3$; and (f) the square to oblique or SO case, driven by ε_2 and ε_3, independently. [The oblique to oblique ferroelastic ($p2$ to $p1$) transition that involves merely a loss of inversion symmetry is not considered (Ref. 35).]

We neglect ''geometric'' nonlinearity, as justified by the scaling of Appendix B, where such corrections are higher order in a typical (small) strain value. We notationally distinguish between OP strains $\{\varepsilon_\ell\}$ and non-OP strains $\{e_i\}$. The potential $V=F(\{\varepsilon_\ell\})+f(\{e_i\})$ is anharmonic through F in the N_{op} order-parameter strains, and harmonic through f in the n non-OP strains, while the Rayleigh dissipation $R^{tot}(\{\dot{\varepsilon}_\ell\},\{\dot{e}_i\})$ is harmonic in both the strain rates,

$$f=\sum_{\vec{r},i}\frac{1}{2}a_i e_i^2, \quad R^{tot}=\sum_{\vec{r},\ell}\frac{1}{2}A'_\ell\dot{\varepsilon}_\ell^2+\sum_{\vec{r},i}\frac{1}{2}a'_i\dot{e}_i^2. \quad (2.3)$$

Here, as in Appendix B, $\{A_\ell\},\{a_i\}$ and $\{A'_\ell\},\{a'_i\}$ are, respectively, OP and non-OP second-order elastic and friction coefficients, and the sum is over sites $\{\vec{r}\}$ of a reference lattice, while t is a scaled time.

TR dynamics from displacement variation

Consider the TR transition, for which $N_{op}=2$ and $n=1$. Figure 1 shows the TR, the SR, and other lattice transitions. (While it is true[16,17] that these correspond to 2D projections/analogs of hexagonal to orthorhombic, and tetragonal to orthorhombic lattice transitions, respectively, we will reserve this 3D terminology for full 3D analyses, elsewhere.) The symmetry-adapted non-OP compressional strain $e_1=\frac{1}{2}(\Delta_x u_x+\Delta_y u_y)$, whereas the OP are the ''deviatoric'' $\varepsilon_2=\frac{1}{2}(\Delta_x u_x-\Delta_y u_y)$ and shear strain $\varepsilon_3=\frac{1}{2}(\Delta_x u_y+\Delta_y u_x)$. The deviatoric strain can be regarded as a simple shear rotated by $\pi/4$.

Then Eq. (2.3) for the non-OP compressional energy is $f=\Sigma_{\vec{r}}\frac{1}{2}a_1 e_1^2, R^{tot}=\frac{1}{2}\Sigma_{\vec{r}}[a'_1\dot{e}_1^2+(A'_2\dot{\varepsilon}_2^2+A'_3\dot{\varepsilon}_3^2)]$. The anharmonic and fourth-order (triple-well) free energy F for ε_2, ε_3, is given below in Eq. (3.27a), although this explicit form is not needed in the derivation.

Defining OP free-energy derivatives (i.e., stresses) $F_{2,3}\equiv\delta F/\delta\varepsilon_{2,3}(r,t)$, the Lagrange-Rayleigh variation with respect to displacements $\vec{u}(\vec{r},t)$ gives for the dynamics of Eq. (2.1)

$$\rho_0\ddot{u}_x=\frac{1}{2}[a_1\Delta_x e_1+\Delta_x F_2+\Delta_y F_3]+\frac{1}{2}[a'_1\Delta_x\dot{e}_1+A'_2\Delta_x\dot{\varepsilon}_2+A'_3\Delta_y\dot{\varepsilon}_3], \quad (2.4a)$$

$$\rho_0\ddot{u}_y=\frac{1}{2}[a_1\Delta_y e_1-\Delta_y F_2+\Delta_x F_3]+\frac{1}{2}[a'_1\Delta_y\dot{e}_1-A'_2\Delta_y\dot{\varepsilon}_2+A'_3\Delta_x\dot{\varepsilon}_3]. \quad (2.4b)$$

These displacement equations have been obtained previously,[16] but were then truncated by dropping the displacement acceleration (second time derivative) to yield reduced equations that are analyzed further in Appendix C. Instead, we pursue here the underdamped OP-strain equations and find they have a generalized BG form.

The strains obey the compatibility constraints, which in the displacement picture ensure that $\vec{u}$ is single valued (i.e., cross-derivatives commute). The equation for the 2D case is, at every instant,

$$\vec{\Delta}^2 e_1-(\Delta_x^2-\Delta_y^2)\varepsilon_2-2\Delta_x\Delta_y\varepsilon_3=0. \quad (2.5)$$

Taking spatial derivatives of Eq. (2.4) we obtain the full underdamped equations for the strains,

$$\rho_0\ddot{e}_1=\frac{1}{4}\left[a_1\vec{\Delta}^2 e_1+(\Delta_x^2-\Delta_y^2)\frac{\partial F}{\partial\varepsilon_2}+2\Delta_x\Delta_y\frac{\partial F}{\partial\varepsilon_3}\right]+\frac{1}{4}[a'_1\vec{\Delta}^2\dot{e}_1+A'_2(\Delta_x^2-\Delta_y^2)\dot{\varepsilon}_2+2A'_3\Delta_x\Delta_y\dot{\varepsilon}_3], \quad (2.6a)$$

$$\rho_0\ddot{\varepsilon}_2=\frac{1}{4}\left[a_1(\Delta_x^2-\Delta_y^2)e_1+\vec{\Delta}^2\frac{\partial F}{\partial\varepsilon_2}\right]+\frac{1}{4}[a'_1(\Delta_x^2-\Delta_y^2)\dot{e}_1+A'_2\vec{\Delta}^2\dot{\varepsilon}_2], \quad (2.6b)$$

$$\rho_0\ddot{\varepsilon}_3=\frac{1}{4}\left[2a_1\Delta_x\Delta_y e_1+\vec{\Delta}^2\frac{\partial F}{\partial\varepsilon_3}\right]+\frac{1}{4}[2a'_1\Delta_x\Delta_y\dot{e}_1+A'_3\vec{\Delta}^2\dot{\varepsilon}_3]. \quad (2.6c)$$

By taking appropriate derivatives of Eq. (2.6), it is easy to see that the compatibility condition (2.5) is satisfied as an identity. This *linear* equation, Eq. (2.5), can then be used

instead of the nonlinear Eq. (2.6a), to eliminate the non-OP strain $e_1(\vec{k},\omega)$ in terms of the OP strains $\varepsilon_{2,3}(\vec{k},\omega)$, assuming periodic boundary conditions.

Defining $a_{1\omega}\equiv a_1-i\omega a_1'$, transforming to Fourier space, and with $F_{2,3}$ now defined as $F_{2,3}\equiv\partial F/\partial\varepsilon^*_{2,3}(\vec{k},\omega)$, the compatibility constraint (2.5),

$$Q_1 e_1(\vec{k},\omega)+Q_2\varepsilon_2(\vec{k},\omega)+Q_3\varepsilon_3(\vec{k},\omega)=0, \qquad (2.7)$$

with $Q_1\equiv -k^2, Q_2\equiv k_x^2-k_y^2, Q_3\equiv 2k_xk_y$, is used to eliminate $e_1(\vec{k},\omega)$, giving $N_{OP}=2$ order-parameter strain-only equations,[31]

$$\rho_0\omega^2\varepsilon_2=\frac{k^2}{4}\left[a_{1\omega}\left(\frac{Q_2^2}{Q_1^2}\varepsilon_2+\frac{Q_2Q_3}{Q_1^2}\varepsilon_3\right)+F_2-i\omega A_2'\varepsilon_2\right], \qquad (2.8a)$$

$$\rho_0\omega^2\varepsilon_3=\frac{k^2}{4}\left[a_{1\omega}\left(\frac{Q_2Q_3}{Q_1^2}\varepsilon_2+\frac{Q_3^2}{Q_1^2}\varepsilon_3\right)+F_3-i\omega A_3'\varepsilon_3\right]. \qquad (2.8b)$$

These can be succinctly written as an OP dynamics for $\varepsilon_\ell(r,t)$ with $(\ell=2,3)$,

$$\rho_0\ddot{\varepsilon}_\ell=\frac{1}{4}\vec{\Delta}^2\left(\frac{\delta(F+F^c)}{\delta\varepsilon_\ell}+\frac{\delta(R+R^c)}{\delta\dot{\varepsilon}_\ell}\right), \qquad (2.9)$$

where F^c and R^c are compatibility-induced contributions from the non-OP free energy f and dissipation R written in terms of the OP strains,

$$F^c=\frac{1}{2}a_1\sum_{\vec{k},\ell,\ell'}U^c_{\ell\ell'}(\hat{k})\varepsilon_\ell(\vec{k},t)\varepsilon^*{}_{\ell'}(\vec{k},t), \qquad (2.10a)$$

$$R^c=\frac{1}{2}a_1'\sum_{\vec{k},\ell,\ell'}\eta^c_{\ell\ell'}(\hat{k})\dot{\varepsilon}_\ell(\vec{k},t)\dot{\varepsilon}^*{}_{\ell'}(\vec{k},t), \qquad (2.10b)$$

where the orientation-dependent kernel[31] $U^c_{\ell\ell'}(\hat{k})=\eta^c_{\ell\ell'}(\hat{k})$ is defined implicitly above, and given explicitly in Eq. (3.29) of Sec. III, following a strain-based derivation of the same dynamics.

The system of $N_{op}=2$ underdamped equations (2.9) derived for the strains is clearly of a Bales-Gooding form [compare with Eq. (1.1)], but now generalized in three ways: by the derived replacement $\partial^2/\partial x^2\to\vec{\Delta}^2$; by the appearance of a compatibility-induced (ALR) interaction, between ε_ℓ-$\varepsilon_{\ell'}$ (and not ε_ℓ^2-$\varepsilon_{\ell'}^2$); and of a similiar compatibility-induced ALR dissipation, between $\dot{\varepsilon}_\ell$-$\dot{\varepsilon}_{\ell'}$ strain rates.

An interesting consequence of the BG structure with periodic boundary conditions is that the "$\vec{k}=0$" (or more precisely, $\vec{k}\to 0$) OP strain obeys $\rho_0\ddot{\varepsilon}_\ell(\vec{k}=0,t)=0$, so macroscopic strain momentum $\rho_0\dot{\varepsilon}_\ell(\vec{k}=0,t)=0$ is conserved,[33] unaffected by internal forces and dissipations. The solution is $\varepsilon_\ell(\vec{k}=0,t)=\dot{\varepsilon}_\ell(\vec{k}=0,0)t+\varepsilon_\ell(\vec{k}=0,0)$. In the special case of an austenite phase with initial conditions $\dot{\varepsilon}_\ell(\vec{k}=0,0)=0$, and $\varepsilon_\ell(\vec{k}=0,0)\sim\Sigma_r\varepsilon_\ell(r,0)=0$, strains of *both* signs will develop on cooling below transition, as a consequence of the dynamics. The OP strain is in this case like a "charge" that is generated in sign-balancing pairs, and the notion of elastic "screening" helps in understanding simulations presented later.

The SR dynamics, driven by a deviatoric strain OP, can similiarly be shown by displacement variation to be also of the generalized BG form, as given in the first part of Appendix A. However, we now proceed to derive the strain dynamics through strain variation.

III. OP STRAIN DYNAMICS BY STRAIN VARIATION WITH COMPATIBILITY CONSTRAINTS

In discussions of ferroelastics, it is common to assert that although the free energy is in terms of the strains, the true basic variables for such systems are displacements, since strains are just displacement derivatives. Thus Monte Carlo simulations, numerical solutions of dynamic equations, and static analyses of textures, even when expressed in terms of strains, are all finally performed in terms of displacements. Following the electromagnetic analogy mentioned in the Introduction, an alternative treatment is in terms of *strains* as the basic variables. The free energy for a first-order transition, say, $F_0\sim\varepsilon^6$, is then regarded as zeroth order in derivatives, whereas in the displacement picture it is a sixth power of derivatives. In this section, we derive ferroelastic dynamics for the TR and SR cases, using strains as the variational quantities. Results for external stress and noise are also stated. We use periodic boundary conditions throughout[33,34] and transform between coordinate $\vec{r}$ and wave vector $\vec{k}$ descriptions, as convenient. The Lagrange-Rayleigh dynamics equation for a general variable α is

$$\frac{d}{dt}\frac{\partial L}{\partial\dot{\alpha}}-\frac{\partial L}{\partial\alpha}=-\frac{\partial R^{tot}}{\partial\dot{\alpha}}, \qquad (3.1)$$

and we consider here the strains as the variables,

$$\alpha\to\{E_{\mu\nu}(\vec{r},t)\}. \qquad (3.2)$$

In total, if we consider all space groups in two dimensions, there are 23 ferroelastic transitions[35] in two dimensions. Figure 1 shows the six symmetry-allowed transitions in two dimensions for the four crystal systems with monatomic basis. We will present the initial part of the argument in general form, before focusing on the triangular to (centered) rectangular lattice or TR case; and the square to rectangle or SR case, with other 2D transitions considered in Sec. VI.

The Lagrangian contains the potential V and kinetic energy T that depend on symmetry-adapted strains which are the basis functions of irreducible representations of the unit-cell symmetry group. In general, these are linear combinations of the strain tensor $\{E_{\mu\nu}\}$. The $s=1,2,\ldots,N$ symmetry-adapted strains are written as $\{e_s\}$, with $N=3$ in two dimensions (and 6 in three dimensions). In two dimensions, except for the RO case, the compressional (e_1), deviatoric (e_2), and shear (e_3) strains are defined by

$$\frac{e_1}{c_1}=\frac{1}{2}(E_{xx}+E_{yy}), \quad \frac{e_2}{c_2}=\frac{1}{2}(E_{xx}-E_{yy}),$$

$$\frac{e_3}{c_3}=\frac{1}{2}(E_{xy}+E_{yx}), \tag{3.3}$$

where c_1, c_2, c_3 are symmetry-specific constants.

The strain tensor (neglecting geometric nonlinearity as justified in Appendix B) obeys the St. Venant compatibility condition, which is here a field equation forbidding defects such as dislocations and vacancies[29,30] at every instant,

$$\vec{\Delta}\times[\vec{\Delta}\times\underset{=}{\mathbf{E}}(\vec{r},t)]^T=0, \tag{3.4a}$$

$$\vec{k}\times\underset{=}{\mathbf{E}}(\vec{k},t)\times\vec{k}=0, \tag{3.4b}$$

with no source term on the right-hand side. The $p=1,2,\ldots,N_c$ compatibility conditions are

$$C^{(p)}\equiv\sum_s \hat{Q}_s^{(p)} e_s(\vec{r},t)=0, \tag{3.5}$$

where $\hat{Q}_\mu^{(p)}$ are second-order derivative operators, from Eq. (3.4a). In two dimensions there is only one compatibility equation $N_c=1$, and the operators in Fourier space are $Q_1(\vec{k})\equiv-\vec{k}^2/c_1$, $Q_2(\vec{k})\equiv(k_x^2-k_y^2)/c_2$, $Q_3(\vec{k})\equiv 2k_xk_y/c_3$. Thus Eq. (3.5) for $e_s(\vec{k},t)$ is, from Eq. (3.4b),

$$Q_1e_1+Q_2e_2+Q_3e_3=0. \tag{3.6}$$

The anisotropic compatibility factors $Q_{1,2,3}(\vec{k})$ encode the discrete symmetries of the compressional, deviatoric, and shear strains. The symmetry constants for the TR case are $c_1=c_2=c_3=1$, whereas for the SR case they are $c_1=c_2=\sqrt{2}, c_3=1$. The compatibility constraint will be invoked repeatedly in the derivations below. The physical meaning of the constraint is that order parameter strains should not tear, or cause defects in the lattice, i.e., lattice integrity is maintained. Suppose, in a sea of square unit cells, one cell was made rectangular (local deviatoric strain). It is clear that in order to maintain lattice integrity, the neighboring cells must also deform, inducing all three strains in an interrelated way, with a similar (but smaller) deformation of the larger number of further neighbors. The requirement of a smooth, compatible fitting together of neighboring unit cells will cause the disturbance to propagate outwards, and in an anisotropic way (due to discrete crystal symmetry and elastic constants): the *local* condition has *global* consequences.

The Lagrangian L also contains the compatibility constraints through dynamic Lagrange multipliers $\{\Lambda^{(p)}(\vec{r},t)\}$,

$$L=\int dt\left[T-V-\sum_{p,\vec{r}}\Lambda^{(p)}C^{(p)}\right]. \tag{3.7}$$

We now (a) obtain the kinetic energy $T(\{\dot{e}_\mu\})$ in terms of the time derivatives of the symmetry-adapted strains; and (b) use this to derive the TR and SR dynamics by strain variation, incorporating the compatibility constraint.

A. Kinetic energy in terms of strain rates

Since Newtonian dynamics is for *point* particles, the kinetic energy in terms of displacements is

$$T=\frac{1}{2}\rho_0\sum_{\vec{r},\mu}\dot{u}_\mu^2(\vec{r},t)=\frac{1}{2}\rho_0\sum_{\vec{k},\mu}|\dot{u}_\mu(\vec{k},t)|^2 \tag{3.8}$$

in coordinate and wave-vector spaces, where ρ_0 is a dimensionless mass density that is a ratio of typical kinetic and elastic energy densities (Appendix B). In the strain picture, the displacement can be defined in terms of the strains through the Kirchhoff-Cesaro-Volterra relation[30]

$$\vec{u}(\vec{r})=\int_{C(\vec{r}_o,\vec{r})}[\underset{=}{\mathbf{E}}(\vec{l})+\{(\vec{l}-\vec{r})\times\vec{\nabla}_{\vec{l}}\times\underset{=}{\mathbf{E}}(\vec{l})\}]\cdot d\vec{l}, \tag{3.9a}$$

where the line integral is along any contour $C(\vec{r}_o,\vec{r})$ to $\vec{r}$ from $\vec{r}_o$, which is a fixed point of the deformation. This is valid up to a global translation and a global rotation, that can be viewed as integration constants (taken to vanish for periodic boundary conditions). Therefore, taking derivatives with respect to $\vec{r}$, the symmetric combination is the same as Eq. (2.2) as it must be:

$$\frac{1}{2}(\Delta_\mu u_\nu+\Delta_\nu u_\mu)=E_{\mu\nu}. \tag{3.9b}$$

In two dimensions, two of the displacement gradients can be obtained from Eqs. (2.2) and (3.3) and expressed in terms of order parameter strain symmetry coordinates as

$$\Delta_x u_x=\frac{e_1}{c_1}+\frac{e_2}{c_2}, \quad \Delta_y u_y=\frac{e_1}{c_1}-\frac{e_2}{c_2}. \tag{3.10a}$$

Taking time derivatives and transforming to Fourier space gives for $k_x, k_y\neq 0$,

$$\dot{u}_x(\vec{k},t)=\frac{\dfrac{\dot{e}_1}{c_1}+\dfrac{\dot{e}_2}{c_2}}{ik_x}, \quad \dot{u}_y(\vec{k},t)=\frac{\dfrac{\dot{e}_1}{c_1}-\dfrac{\dot{e}_2}{c_2}}{ik_y}. \tag{3.10b}$$

Inserting Eq. (3.10b) into Eq. (3.8) yields the kinetic energy that is *nonlocal* in terms of the strain rates,

$$T=\sum_{\vec{k},s,s'}\frac{1}{2}\rho_{ss'}(\vec{k})\dot{e}_s^*(\vec{k},t)\dot{e}_{s'}(\vec{k},t)$$

$$=\sum_{\vec{r},\vec{r}',s,s'}\frac{1}{2}\rho_{ss'}(\vec{r}-\vec{r}')\dot{e}_s^*(\vec{r},t)\dot{e}_{s'}(\vec{r}',t), \tag{3.11}$$

where we have introduced an anisotropic ''strain mass-density tensor'' whose components turn out to be related to ratios of the compatibility factors of Eq. (3.6),

$$\rho_{ss'}(\vec{k})=\rho(k)\begin{bmatrix} \frac{1}{c_1^2}\frac{k^2}{k_x^2k_y^2} & -\frac{1}{c_1c_2}\frac{(k_x^2-k_y^2)}{k_x^2k_y^2} \\ -\frac{1}{c_1c_2}\frac{(k_x^2-k_y^2)}{k_x^2k_y^2} & \frac{1}{c_2^2}\frac{k^2}{k_x^2k_y^2} \end{bmatrix}$$

$$=\rho(k)\begin{bmatrix} \left(\frac{Q_1}{Q_3}\right)^2 & \left(\frac{Q_1Q_2}{Q_3^2}\right) \\ \left(\frac{Q_2Q_1}{Q_3^2}\right) & \frac{c_1^2}{c_2^2}\left(\frac{Q_1}{Q_3}\right)^2 \end{bmatrix}. \tag{3.12a}$$

This strain mass-density tensor is a kinematic time-independent quantity true for all 2D symmetries and has a determinant $(2/c_1c_2k_xk_y)^2$. Here

$$\rho(k)\equiv\frac{4\rho_0}{c_3^2k^2} \tag{3.12b}$$

and therefore long-wavelength strains over many lattice spacings are effectively more ''massive,'' as is physically reasonable. In 2D coordinate space, $\rho_{ss'}(\vec{R})\sim(4\rho_0)\ln(|\vec{R}|)$. It is this inverse Laplacian dependence that gives rise to the Bales-Gooding structure (1.3) of the underdamped dynamics. The strain kinetic energy can be expressed only in terms of the compressional and deviatoric strain rates, i.e., the ''shear components'' of the strain mass tensor are zero, $\rho_{s3}=\rho_{3s}=0$. This is because from Eqs. (3.3) and (3.9b), the shear strain rate

$$\frac{\dot{e}_3(\vec{k})}{c_3}=\frac{1}{2}[ik_x\dot{u}_y(\vec{k})+ik_y\dot{u}_x(\vec{k})], \tag{3.13}$$

is not independent, but is related to the other strain rates by a consistency condition through Eq. (3.10b), which turns out to be precisely the compatibility constraint.

B. Dynamics by strain variations

The compatibility conditions (3.5) become

$$C^{(p)}(r,t)=\sum_\ell \hat{Q}_\ell^{(p)}\varepsilon_\ell(\vec{r},t)+\sum_i \hat{Q}_i^{(p)}e_i(\vec{r},t)=0, \tag{3.14a}$$

and therefore in Fourier space

$$C^{(p)}(\vec{k},t)=\sum_\ell Q_\ell^{(p)}(\vec{k})\varepsilon_\ell(\vec{k},t)+\sum_i Q_i^{(p)}(\vec{k})e_i(\vec{k},t)=0. \tag{3.14b}$$

The Gibbs free energy $V(\{\varepsilon_\ell\},\{e_i\})$ depends harmonically on the non-OP strains through f and anharmonically on OP strains through F, whereas the Rayleigh dissipation R^{tot} to the lowest order depends harmonically on all strain rates. Thus,

$$V=f(\{e_i\})+F(\{\varepsilon_\ell\}),\qquad f=\frac{1}{2}\sum_{i,r} a_ie_i^2,$$

$$R^{tot}=\frac{1}{2}\sum_{i,r} a_i'\dot{e}_i^2+\frac{1}{2}\sum_{\ell,r} A_\ell'\dot{\varepsilon}_\ell^2, \tag{3.15}$$

where a_i, a_i' are the non-OP elastic and friction constants.

The kinetic energy in terms of strain rates $\{\dot{e}_i\},\{\dot{\varepsilon}_\ell\}$, from Eq. (3.11), is

$$T=\sum_{\vec{k},\ell,\ell'}\frac{1}{2}\rho_{\ell\ell'}(\vec{k})\dot{\varepsilon}_\ell^*(\vec{k},t)\dot{\varepsilon}_{\ell'}(\vec{k},t)$$
$$+\sum_{\vec{k},i,i'}\frac{1}{2}\rho_{ii'}(\vec{k})\dot{e}_i^*(\vec{k},t)\dot{e}_{i'}(\vec{k},t)\}. \tag{3.16}$$

Using Eqs. (3.14b), (3.15), and (3.16), the Lagrange-Rayleigh dynamics for OP and non-OP strains are given by directly varying the *strains* in Eqs. (3.1) and (3.7),

$$\sum_{\ell'}\rho_{\ell\ell'}\ddot{\varepsilon}_{\ell'}+\sum_{i'}\rho_{\ell i'}\ddot{e}_{i'}=-\frac{\partial F}{\partial\varepsilon_\ell}-\sum_p Q_\ell^{(p)}\Lambda^{(p)}-A_\ell'\dot{\varepsilon}_\ell, \tag{3.17a}$$

$$\sum_{i'}\rho_{ii'}\ddot{e}_{i'}+a_ie_i+a_i'\dot{e}_i+\sum_p Q_i^{(p)}\Lambda^{(p)}=-\sum_{\ell'}\rho_{i\ell'}\ddot{\varepsilon}_{\ell'}, \tag{3.17b}$$

$$\sum_i Q_i^{(p)}e_i=-\sum_\ell Q_\ell^{(p)}\varepsilon_\ell. \tag{3.17c}$$

We have written the equations in a general form for future 3D BG generalizations such as the cubic to tetragonal transition.[11] There are $(n+N_c)$ linear equations (3.17b) and (3.17c) for $(n+N_c)$ variables $\{e_i\},\{\Lambda^{(p)}\}$ that can be written in matrix form, and inverted to yield the dynamics for the OP strains $\{\varepsilon_\ell\}$. We do not pursue this general treatment here, but now specialize to the TR case and give the result for SR case at the end of the section. Other symmetries are considered in Sec. VI.

TR underdamped dynamics

For the TR transition, $n=1, N_{op}=2, N_c=1$; the non-OP strain is compressional e_1; the OP strains are ''deviatoric'' and shear ($\varepsilon_2,\varepsilon_3$ respectively); whereas the symmetry constants of Eq. (3.6) are $c_1=c_2=c_3=1$. The strain mass-density components are $\rho_{11}=\rho(k)(Q_1/Q_3)^2=\rho_{22},\rho_{12}=\rho(k)(Q_1Q_2/Q_3^2)=\rho_{21}$. We have $N_{op}+n+N_c=2+1+1=4$ equations like Eq. (3.17),

$$\rho_{22}\ddot{\varepsilon}_2+\rho_{21}\ddot{e}_1=-\frac{\partial F}{\partial\varepsilon_2^*}-Q_2\Lambda-A_2'\dot{\varepsilon}_2, \tag{3.18a}$$

$$0=-\frac{\partial F}{\partial\varepsilon_3^*}-Q_3\Lambda-A_3'\dot{\varepsilon}_3, \tag{3.18b}$$

$$\rho_{11}\ddot{e}_1+\rho_{12}\ddot{\varepsilon}_2=-a_1e_1-a_1'\dot{e}_1-Q_1\Lambda, \tag{3.18c}$$

$$Q_1e_1=-Q_2\varepsilon_2-Q_3\varepsilon_3. \tag{3.18d}$$

There are $N_{op}=2$ nonlinear equations for $\varepsilon_{2,3}$ and $n+N_c=2$ linear equations for e_1,Λ. We can use the compatibility equation (3.18d) for the strain mass density $\{\rho_{ss'}(\vec{k})\}$ components in Eq. (3.12) to write the expression on the left-hand side of Eq. (3.18c) as

$$\rho_{11}\ddot{e}_1+\rho_{12}\ddot{\varepsilon}_2=\frac{4\rho_0}{Q_3}\ddot{\varepsilon}_3. \tag{3.19}$$

The Lagrange multiplier of Eq. (3.18c) is determined by the OP strains as

$$\Lambda(\vec{k},\omega)=\frac{1}{Q_1^2}\left[a_{1\omega}\varepsilon_2+\left(a_{1\omega}Q_3+\frac{4\rho_0\omega^2Q_1}{Q_3}\right)\varepsilon_3\right], \tag{3.20}$$

where $a_{1\omega}=a_1-i\omega a_1'$. Substituting Eq. (3.20) into Eq. (3.18) with the identity

$$\rho_{22}-\rho_{21}\frac{Q_2}{Q_1}=\frac{4\rho_0}{k^2}, \tag{3.21}$$

yields the TR equations in terms of the OP strains alone,[31]

$$\rho_0\omega^2\varepsilon_2=\frac{k^2}{4}\left[\frac{\delta F}{\delta\varepsilon_2^*}+a_{1\omega}\left(\frac{Q_2^2}{Q_1^2}\varepsilon_2+\frac{Q_2Q_3}{Q_1^2}\varepsilon_3\right)-i\omega A_2'\varepsilon_2\right], \tag{3.22a}$$

$$\rho_0\omega^2\varepsilon_3=\frac{k^2}{4}\left[\frac{\delta F}{\delta\varepsilon_3^*}+a_{1\omega}\left(\frac{Q_2Q_3}{Q_1^2}\varepsilon_2+\frac{Q_3^2}{Q_1^2}\varepsilon_3\right)-i\omega A_3'\varepsilon_3\right]. \tag{3.22b}$$

Since ratios of compatibility factors recur, it is useful to define

$$Q_{\ell,\ell'}(\hat{k})\equiv\frac{Q_\ell(\vec{k})}{Q_{\ell'}(\vec{k})}. \tag{3.23}$$

The non-OP strain in Eq. (3.18d) is a *derived* quantity,

$$\begin{aligned}e_1(\vec{k},\omega)&=-[Q_{2,1}(\hat{k})\varepsilon_2(\vec{k},\omega)+Q_{3,1}(\hat{k})\varepsilon_3(\vec{k},\omega)]\\&\equiv S_{12}\varepsilon_2+S_{13}\varepsilon_3,\end{aligned} \tag{3.24}$$

defining for the TR case, the constants $S_{i\ell}(\hat{k})$ mentioned in Eq. (1.4), which depend only on the wave vector direction $\hat{k}$, i.e., no nontrivial length scale,[31] and not on its magnitude $|\vec{k}|$ (i.e., no length scale).

In a compact form with $\ell=2,3$,

$$\rho_0\omega^2\varepsilon_\ell=\frac{k^2}{4}\left(\frac{\delta(F+F_c)}{\delta\varepsilon_\ell^*(\vec{k},\omega)}+\frac{\delta(R+R^c)}{\delta\dot{\varepsilon}_\ell{}^*(\vec{k},\omega)}\right). \tag{3.25}$$

This is written as an OP strain-only dynamics for $\varepsilon_\ell(\vec{r},t)$,

$$\rho_0\ddot{\varepsilon}_\ell(\vec{r},t)=\frac{1}{4}\vec{\Delta}^2\left(\frac{\delta(F+F^c)}{\delta\varepsilon_\ell(\vec{r},t)}+\frac{\delta(R+R^c)}{\dot{\varepsilon}_\ell(\vec{r},t)}\right), \tag{3.26}$$

which can be written as a strain-momentum continuity equation.[33] The OP free energy from Appendix B is

$$F_0=\sum_{\vec{r}}\left[\frac{K_0}{2}\sum_\ell(\vec{\Delta}\varepsilon_\ell)^2+(\tau-1)(\varepsilon_2^2+\varepsilon_3^2)+\{(\varepsilon_2^2+\varepsilon_3^2)-2(\varepsilon_2^3-3\varepsilon_2\varepsilon_3^2)+(\varepsilon_2^2+\varepsilon_3^2)^2\}\right]. \tag{3.27a}$$

This free energy is invariant under the $6mm$ point group operations. Specifically, under three fold rotations, $E_{x'x'}=E_{xx}/4+3E_{yy}/4+(\sqrt{3}/2)E_{xy}$; $E_{y'y'}=\frac{3}{4}E_{xx}+\frac{1}{4}E_{yy}-(\sqrt{3}/2)E_{xy}$; $E_{x'y'}=-(\sqrt{3}/4)(E_{xx}-E_{yy})-\frac{1}{2}E_{xy}$ and the non-OP and OP strains transform as $e_1'=e_1,\varepsilon_2'=-\frac{1}{2}\varepsilon_2-(\sqrt{3}/2)\varepsilon_3,\varepsilon_3'=(\sqrt{3}/2)\varepsilon_2-\frac{1}{2}\varepsilon_3$. The (anharmonic) OP free energy has not been explicitly used in the derivation of the dynamics, whose structure depends only on the number and nature of the (harmonic) non-OP strains.

The compatibility induced OP-OP interaction is the non-OP free energy written in terms of the OP strains, $f[e_1(\{\varepsilon_\ell\})]\equiv F^c(\{\varepsilon_\ell\})$ with $(\ell=2,3)$,

$$\begin{aligned}F^c&=\frac{1}{2}a_1\sum_{\vec{r},\vec{r}',\ell,\ell'}\varepsilon_\ell(\vec{r},t)U^c_{\ell,\ell'}(\vec{r}-\vec{r}')\varepsilon_{\ell'}(\vec{r}',t)\\&=\frac{1}{2}a_1\sum_{\vec{k},\ell,\ell'}U^c_{\ell,\ell'}(\hat{k})\varepsilon_\ell(\vec{k},t)\varepsilon^*_{\ell'}(\vec{k},t).\end{aligned} \tag{3.27b}$$

The Rayleigh dissipation function for the OP is

$$R=\frac{1}{2}\sum_{\vec{r},\ell}A_\ell'\dot{\varepsilon}_\ell^2, \tag{3.28a}$$

and the compatibility-induced contribution R^c is the non-OP dissipation written in terms of the OP strain rates,

$$\begin{aligned}R^c&=\frac{a_1'}{2}\sum_{\vec{r},\vec{r}',\ell,\ell'}\dot{\varepsilon}_\ell(\vec{r},t)\,\eta^c_{\ell,\ell'}(\vec{r}-\vec{r}')\dot{\varepsilon}_{\ell'}(\vec{r}',t)\\&=\frac{a_1'}{2}\sum_{\vec{k},\ell,\ell'}\eta^c_{\ell,\ell'}(\hat{k})\omega^2\dot{\varepsilon}_\ell(\vec{k},t)\dot{\varepsilon}^*_{\ell'}(\vec{k},t).\end{aligned} \tag{3.28b}$$

Thus, explicitly

$$\frac{\delta(R+R^c)}{\delta\dot{\varepsilon}_\ell^*(\vec{k},\omega)}=\sum_{\ell'}A'_{\ell,\ell'}\dot{\varepsilon}_\ell(\vec{k},\omega), \tag{3.28c}$$

where the effective OP friction is

$$A'_{\ell,\ell'}=A'_\ell\delta_{\ell,\ell'}+a_1'\eta^c_{\ell,\ell'}. \tag{3.28d}$$

Here the (frequency-independent) potential and friction kernels emerging from the dynamics are the same,

$$\eta^c_{\ell\ell'}(\hat{k})=U^c_{\ell\ell'}(\hat{k}), \tag{3.29a}$$

where

$$U^c_{\ell\ell'}=S_{1\ell}S_{1\ell'}=Q_{\ell,1}Q_{\ell',1}\equiv Q_\ell Q_{\ell'}/Q_1^2, \tag{3.29b}$$

and (as from static-constrained minimization),

$$U^c_{22}(\hat{k})=\frac{(k_x^2-k_y^2)^2}{k^4}=(Q_2/Q_1)^2, \tag{3.29c}$$

$$U^c_{33}(\hat{k})=4\frac{k_x^2k_y^2}{k^4}=(Q_3/Q_1)^2,$$

$$U^c_{23}(\hat{k})=\frac{2k_xk_y(k_x^2-k_y^2)}{k^4}=Q_2Q_3/Q_1^2=U^c_{32}(\hat{k}).$$

Both the friction and potential kernels depend on the wavevector direction $\hat{k}$, are independent of $|\vec{k}|$ for long wavelengths,[31] and are ''anisotropic long-range'' functions encoding the discrete symmetry of the lattice, which fall off in coordinate space with a dimensional power, $\eta^c(\vec{R}),U^c(\vec{R})\sim 1/R^D$. At $\vec{k}=0$, the potentials are undefined and we set $U^c_{\ell,\ell'}=0$. (A Coulomb potential, by contrast, diverges for long wavelengths as $\sim 1/k^2$ and falls off as $\sim 1/R^{D-2}$.)

Although Eq. (3.26), derived from strain variation will give the same results as Eq. (2.4), derived from displacement variation, they are conceptually distinct. In the displacement picture, Eq. (2.8), or any equation obtained from it, is solved with (u_x,u_y) on a lattice, with both initial and boundary conditions applied to the basic variables $\vec{u}$. Strains are defined as derivatives of the basic variables, and are derived quantities, e.g., $F\sim\varepsilon_\ell^4$ is a fourth power of derivatives. By contrast, Eq. (3.26) is an OP-strain-only dynamics, and is solved in the strain picture, with $\varepsilon_2,\varepsilon_3$ on a lattice; with initial and boundary conditions applied to the basic variables $\{\varepsilon_\ell\}$; and with the $F\sim\varepsilon_\ell^4$ term as zeroth order in derivatives. (Indeed, the highest-order derivatives are strain-gradient squared or Ginzburg terms.) The non-OP strain is a derived quantity, obtained after solving for the OP and then using Eq. (3.24), the displacement can also, in principle, be derived using Eq. (3.9).

In displacement-picture simulations, terms of the Landau free energy and Rayleigh dissipation are all anisotropic, being powers of the various displacement-derivative combinations. In strain-picture simulations, the anisotropy is in the symmetry-specific compatibility kernels, with OP strains numerically treated as isotropic ''scalars.'' The strain picture has advantages, as it works directly with the physical strain variables, and uses compatibility kernels evaluated once and for all, which encode the unit-cell symmetries and give insight into energetically favored textures.

SR underdamped dynamics

We now turn to the square-rectangle or SR case, which shows a different structure, namely, *time-retarded* OP potentials and friction. For the SR case, $n=2,N_{op}=1,N_c=1$; the non-OP strains are compression and shear e_1, e_3; the OP strain is deviatoric ε_2; the symmetry constants are $c_1=c_2=\sqrt{2},c_3=1$. The compatibility factors are $Q_1(\vec{k})=-k^2/\sqrt{2},Q_2=(k_x^2-k_y^2)/\sqrt{2},Q_3=2k_xk_y$. Then the compatibility constraint (3.6) becomes[10,24]

$$k^2e_1-\sqrt{8}k_xk_ye_3-(k_x^2-k_y^2)\varepsilon_2=0. \tag{3.30}$$

The strain mass components are $\rho_{11}=\rho(k)(Q_1/Q_3)^2=\rho_{22}$, $\rho_{12}=\rho(k)Q_1Q_2/Q_3^2=\rho_{21}$. We have $n+N_{op}+N_c=2+1+1=4$ equations like Eq. (3.17), and with arguments similiar to the TR case we have, from the second part of Appendix A, Eqs. (A9) for ε_2,e_1,e_3,

$$\rho_{22}\ddot{\varepsilon}_2+\rho_{21}\ddot{e}_1=-\frac{\delta F}{\delta\varepsilon_2^*}-Q_2\Lambda-A_2'\dot{\varepsilon}_2, \tag{3.31a}$$

$$0=-a_3e_3-a_3'\dot{e}_3-Q_3\Lambda, \tag{3.31b}$$

$$\rho_{11}\ddot{e}_1+\rho_{12}\ddot{\varepsilon}_2=-a_1e_1-a_1'\dot{e}_1-Q_1\Lambda, \tag{3.31c}$$

$$Q_1e_1+Q_3e_3=-Q_2\varepsilon_2. \tag{3.31d}$$

Substituting for the compressional strain e_1 yields coupled equations between e_3 and ε_2. As in Eq. (3.23), it is convenient to define a variable for the ubiquitous Q ratios, through $Q_{\ell,\ell'}\equiv Q_\ell/Q_{\ell'}$. Then,

$$\rho_0\ddot{\varepsilon}_2=-\frac{c_2^2\vec{k}^2}{4}[Q_{2,1}Q_{3,1}(a_1e_3+a_1'\dot{e}_3)+(a_1Q_{2,1}^2\varepsilon_2+F_2)+(a_1'Q_{2,1}^2+A_2')\dot{\varepsilon}_2], \tag{3.32a}$$

$$\rho_0\ddot{e}_3=-\frac{c_3^2\vec{k}^2}{4}[Q_{2,1}Q_{3,1}(a_1\varepsilon_2+a_1'\dot{\varepsilon}_2)+(a_3+a_1Q_{3,1}^2)e_3+(a_3'+a_1'Q_{3,1}^2)\dot{e}_3]. \tag{3.32b}$$

Eliminating e_3, these yield the final result (A15) in terms of the OP strain alone,

$$\rho_0\omega^2\varepsilon_2=\frac{c_2^2k^2}{4}\left[\frac{\delta F}{\delta\varepsilon_2^*}+a_{1\omega}\frac{b_\omega(Q_2/Q_3)^2}{B_\omega}\varepsilon_2-i\omega A_2'\varepsilon_2\right]. \tag{3.33}$$

As $b_\omega\equiv[a_{3\omega}-(4\rho_0\omega^2/c_3^2k^2)]/a_{1\omega}$, where $a_{i\omega}\equiv a_i-i\omega a_i'$, the kernel is now frequency dependent, and complex, as is the connection (A13) to non-OP strains,

$$e_1=S_{12}\varepsilon_2,\quad S_{12}\equiv-\frac{(Q_1Q_2/Q_3^2)}{B_\omega}b_\omega, \tag{3.34a}$$

$$e_3=S_{32}\varepsilon_2,\quad S_{32}\equiv-\frac{(Q_2/Q_3)}{B_\omega}, \tag{3.34b}$$

where $B_\omega\equiv 1+b_\omega(Q_1/Q_3)^2$. The compatibility condition is manifestly satisfied as an identity.

It is convenient to write the second term on the right-hand side of Eq. (3.33) in terms of real and imaginary parts,

$$\frac{a_{1\omega}b_{\omega}\left(\frac{Q_2}{Q3}\right)^2}{B_{\omega}} \equiv a_1 U^c\left[\hat{k},\omega^2,\left(\frac{\omega}{k}\right)^2\right] - i\omega a_1' \eta^c\left[\hat{k},\omega^2,\left(\frac{\omega}{k}\right)^2\right], \tag{3.35}$$

with U^c, η^c given explicitly later. With this separation,

$$\rho_0\omega^2\varepsilon_2 = \frac{c_2^2}{4}k^2\left[\frac{\delta(F+F^c)}{\delta\varepsilon_2^*(\vec{k},\omega)} + \frac{\delta(R+R^c)}{\delta\dot{\varepsilon}_2^*(\vec{k},\omega)}\right], \tag{3.36}$$

where $c_2^2=2$. The OP dynamics for $\varepsilon_2(\vec{r},t)$ is then

$$\rho_0\ddot{\varepsilon}_2(\vec{r},t) = \frac{1}{2}\vec{\Delta}^2\left[\frac{\partial(F+F^c)}{\partial\varepsilon_2(\vec{r},t)} + \frac{\partial(R+R^c)}{\partial\dot{\varepsilon}_2(\vec{r},t)}\right], \tag{3.37}$$

where the OP triple-well free energy is the same as in Appendix B,

$$F_0 = \sum_{\vec{r}} (\tau-1)\varepsilon_2^2 + \varepsilon_2^2(\varepsilon_2^2-1)^2 + \frac{K_0}{2}(\vec{\Delta}\varepsilon_2)^2. \tag{3.38a}$$

Under fourfold rotations, $E_{xx}\to E_{yy}, E_{yy}\to E_{xx}, E_{xy}\to -E_{xy}$, the non-OP and OP strains transform as $e_1\to e_1, e_2\to -\varepsilon_2, e_3\to -e_3$, leaving the free energy invariant and similarly for other $4mm$ point group operations. The (anharmonic) OP free energy F_0 is not explicitly used in the derivation, and the dynamics depends only on the number and type of the non-OP strains.

We note that ω dependences carry an infinitesimal imaginary part to maintain causality, and thus Eq. (3.37) has contributions only from earlier times,

$$\frac{\partial F^c}{\partial\varepsilon_2} = a_1\int_{-\infty}^{t} dt' \sum_{\vec{r}'} U^c(\vec{r}-\vec{r}', t-t')\varepsilon_2(\vec{r}', t'). \tag{3.38b}$$

The OP dissipation in addition to

$$R = \frac{1}{2}\sum_{\vec{r}} A_2'\dot{\varepsilon}_2^2, \tag{3.39a}$$

now also has a retarded compatibility contribution,

$$\frac{\partial R^c}{\partial\dot{\varepsilon}_2} = a_1'\int_{-\infty}^{t} dt' \sum_{r'} \eta^c(\vec{r}-\vec{r}', t-t')\dot{\varepsilon}_2(\vec{r}', t'). \tag{3.39b}$$

Both are ALR functions $U^c, \eta^c \sim 1/R^D$ as before but are also *retarded in time*. For negligible non-OP friction $a_1'=a_3'=0$, the compatibility-induced friction vanishes, $a_1'\eta^c=0$. The non-OP compressional and shear strains $e_{1,3}(\vec{r},t)$ are *derived* quantities obtained after solving for $\varepsilon_2(\vec{r},t)$ and using Eq. (3.34), and the constants $S_{i\ell}$ are frequency-dependent and therefore retarded in time, like the compatibility potential.

The real and imaginary parts of the kernel of Eq. (3.35) that give rise to the compatibility-induced OP potential U^c and the friction coefficient η^c are explicitly

$$U^c(\hat{k},\omega^2,v^2) = \frac{a_3}{a_1}Q_{2,3}^2\frac{\left[1+\frac{a_1}{a_3}|b_{\omega}|^2Q_{1,3}^2\right]}{[(1+b_rQ_{1,3}^2)^2+b_i^2Q_{1,3}^4]}, \tag{3.40a}$$

where the "velocity" $v\equiv\omega/k$, and

$$b_r \equiv \frac{a_3}{a_1}\frac{\left(g+\omega^2\frac{a_1'}{a_1}\frac{a_3'}{a_3}\right)}{\left[1+\left(\frac{\omega a_1'}{a_1}\right)^2\right]}, \quad b_i \equiv \frac{\frac{a_3}{a_1}\omega\left[g\frac{a_1'}{a_1}-\frac{a_3'}{a_3}\right]}{\left[1+\left(\frac{\omega a_1'}{a_1}\right)^2\right]},$$

$$|b_{\omega}|^2 \equiv b_r^2+b_i^2 = \left(\frac{a_3}{a_1}\right)^2\frac{\left[g^2+\left(\frac{\omega a_3'}{a_3}\right)^2\right]}{\left[1+\left(\frac{\omega a_1'}{a_1}\right)^2\right]}. \tag{3.40b}$$

Similarly,

$$\eta^c(\hat{k},\omega^2,v^2) = \frac{(Q_{1,3}Q_{2,3})^4|b_{\omega}|^2+\frac{a_3'}{a_1'}(Q_{2,3})^4}{[(1+b_rQ_{1,3}^2)^2+b_i^2(Q_{1,3})^4]}, \tag{3.40c}$$

with

$$g \equiv 1-\frac{4\rho_0}{c_3^2a_3}\left(\frac{\omega}{k}\right)^2. \tag{3.40d}$$

Note that both the static and dynamic U^c are zero for diagonal orientations, when $Q_2=0$. The zero-frequency limit $U^c(\hat{k},0,0)\equiv U_0^c(\hat{k})$ is the static bulk compatibility potential[10,24] used in earlier TDGL simulations,[10] and is

$$U_0^c(\hat{k}) = Q_{2,1}^2/[1+(a_1/a_3)Q_{3,1}^2]. \tag{3.41a}$$

This favors diagonal $k_x/k_y=\pm 1$ textures (when $Q_2=0$), and the derived non-OP strains e_1, e_2 are expelled in a kind of "elastic Meissner effect,"[10] as can be seen from Eq. (3.34). The bulk static compatibility potential is independent of $|\vec{k}|$ for long wavelengths and does not set a domain-wall separation length scale. Near the center point (Γ) of the Brillouin zone (BZ) the $U_0^c(\hat{k})$ depends only on the wave vector direction. It is only in combination with the surface compatibility potential[34] $U^{surface}(k)\sim 1/k$ that equal-width "true" twins (that satisfy a width-length scaling[20,21]) are obtained.[10]

An exact Fourier transform to coordinate space[36] confirms this preference for diagonal orientations: with $\cos\theta=\hat{r}\cdot\hat{r}'$, the coordinate space compatibility potential

$$U_0^c(\vec{r}-\vec{r}') = \frac{G(\theta)}{|\vec{r}-\vec{r}'|^2} \tag{3.41b}$$

is found to have in the prefactor, a basic four-lobe structure from $\cos 4\theta$, with higher harmonics. With $a\equiv 8a_1/a_3$,

$$G(\theta)\equiv\frac{\left[5\cos 4\theta\left(1+\frac{\sin 2\theta}{5}\right)+\left(17+4\frac{a^2}{1+a^2}\right)\sin 2\theta+\left(13-4\frac{a^2}{1+a^2}\right)\right]}{16\sqrt{(1+a^2)}\left(1+\frac{a^2}{1+a^2}\cos 2\theta\right)^2}. \tag{3.41c}$$

Figure 9 in Appendix C (TDGL dynamics), with a single-site initial condition, clearly shows multi-lobe strain textures from these higher harmonics.

Returning to the dynamic case, we see from Eq. (3.40) that the repulsive kernel has a *velocity-resonant structure* through $b_r \simeq g = 1-(v/v_0)^2$, strongest at a propagation speed $v=v_0=\sqrt{a_3/4\rho_0}$, or a time-dependent propagation length scale $L_p(t)=t/t_p$ with $t_p=(4\rho_0/a_3)^{1/2}$. These non-OP inertial effects, with anisotropic directional modulation or finite-velocity retardation $\sim(\omega/k)^2$, compete with frictional delays $\sim\omega^2$, with the peaks becoming singular for vanishing friction. This is somewhat like electrons interacting by exchanging a photon, where the finiteness of the speed of light produces retarded Coulomb potentials.[37] The resonant structure can be thought of as the OP strain textures ''exchanging a non-OP phonon mode,'' causing inertial time delays. $L_p(t)$ is the time-dependent size of an expanding anisotropic ''region of influence'' within which changes in texturing at one point enforce compatible changes in texturing at other points of the lattice. This phonon mediation is also described by the equivalent instantaneous dynamics of Eq. (3.32) with deviatoric and shear strains obeying two coupled underdamped equations, which are convenient for numerical simulations.[38]

The anisotropic potential kernel, $U^c[\hat{k},\omega^2,(\omega/k)^2]$, is plotted in Fig. 2. This shows plots of the kernel versus scaled velocity, namely, $\overline{v}\equiv\sqrt{4\rho_0/a_3}v$ and various BZ wave-vector directions[31] $\alpha=k_x/k_y$ for scaled frequencies $\overline{\omega}^2 \equiv\omega[(a'/a)]^2=0.1$, where we take $a_1'/a_1=a_3'/a_3\equiv a'/a$. U^c determines the positive energy costs of the non-OP strains, which the system wants to eliminate. The smallest U^c is at diagonal texturing $|\alpha|=1$, and zero velocity, $v=0$. The most-non-optimal strains are the most strongly driven, with large U^c. The striking features of Fig. 2 are clearly a preferred diagonal orientation $\alpha=\pm 1$, and a strongest-repulsion textural velocity comparable to sound speeds, $\sim\sqrt{(a_3/4\rho_0)[1+a_1/2a_3]}$ in the ferroelastic material at long times. An extremal textural profile $\varepsilon_2(\vec{k},\omega)$ in Fourier space, if determined from an effective Lagrangian whose variation yields Eq. (3.36), will be shaped by this peaked structure. This suggests that textures will tilt diagonally and thereafter remain stationary and rigid; and that the most unstable or strongest-driven transient interfaces between phases will move/grow at a constant velocity close to the speed of sound.

A fuller investigation of possible evolutions, with intermediate states that can be sensitive to elastic and frictional parameters, requires further work. Here we will only illustrate the rich variety of texturings, and later outline a tentative scenario for nucleation and growth.

Figures 3 and 4 illustrate SR case simulations[39] under the BG-equivalent dynamics of Eq. (3.32), with red, green, and blue representing positive, zero, and negative strains, respectively, with relative color intensities. Parameters are in the captions and quenches are into the martensitic regime $\tau=-0.25$. Figure 3 shows time sequences of BG dynamics for the OP deviatoric strain and the non-OP shear strain. Note the grain-boundary-like regions that rapidly anneal out by tip growth, carrying the shear strain that is already expelled from the diagonal-domain regions. For these parameters, the propagation time $t_p<t_D$; the unit-cell relaxation time is defined later. Figure 4 shows the time sequences, for smaller elastic constants (and hence smaller shear mode velocities/larger propagation times), so $t_p>t_D$. We now have domain walls propagating away from each other, giving the effect of a ''zoom lens'' moving in. Note the non-OP shear fronts moving with the OP walls (compare with Fig. 6). Microstructure as shown in Fig. 3 has been seen in FePd using phase-contrast microscopy,[22] and twinning waves have been found in 1D models.[5]

For parameters as in Fig. 4 and for an intermediate temperature, $\tau=0.85$, Fig. 5 shows dynamical stress responses to applied static deviatoric stress $P_2(r)=P_0/[1+(r/r_0)^2]$, where $r_0=1$ is the width and $P_0=1$ is a time-independent strength. The single-sign induced strain has a large energy, and the system elastically screens it by nucleating hierarchical opposite-sign elastic multipoles, with the propagation length setting a scale, and wave fronts moving out. A sinusoidally time-varying $P_0(t)$ can produce even more striking propagating patterns. Similar ''elastic photocopying'' was found previously using TDGL dynamics, with the surface compatibility potential[10,34] setting a domain-wall separation scale.[40,41]

The last BG simulation[39] of Fig. 6 shows, for the TR case and Eq. (3.26), plots of the OP shear ε_2, with star-triangle patterns as found by other dynamics[16,42,43] and seen experimentally in crystals of lead orthovanadate, $Pb_3(VO_4)_2$, which undergoes a trigonal to monoclinic transition,[44] see also Fig. 8. Once again, the e_1 plot shows that equilibration involves expelling non-OP strains (except at OP corners, with e_1 globally vanishing).

Finally, we note that linearizing the BG dynamics (3.36) about equilibrium in the zero-damping limit yields the familiar wave equation. ''Textural phonon'' spectra can emerge. For a finite $L_0\times L_0$ system we can also include surface-compatibility restoring forces, with a kernel,[10] $U^{surface}$

$\sim(a_3/a_1L_0)/|\vec{k}|$. The long-wavelength OP strain oscillations then have velocities $\omega(\vec{k})/k=v(\hat{k})$ that are obtained by solving

$$v^2\sim\frac{1}{2\rho_0}[\langle F''\rangle+a_1U^c+a_1U^{surface}], \tag{3.42}$$

where $\langle F''\rangle$ is a free-energy curvature averaged with a probability distribution peaked at the equilibrium structure. For infinite systems the long-wavelength spectrum is linear. For finite L_0, very long wavelengths probe the system size,[21] and $\omega\sim(|k|/L_0)^{1/2}$. This is the ''dyadon spectrum''[21] of waves in twin bands of martensite. Anomalies have indeed been observed[45] in some ferroelastic phonon spectra. However, we do not pursue this conjectured explanation here.

C. External stress and noise terms

We now consider stress $\{p_s(\vec{r})\}$ and delta-correlated noise $\{\tilde{g}_s(t)\}$, which modify the free energy as

$$F\to F-\sum_{\ell,\vec{r}}(p_\ell\varepsilon_\ell+\tilde{g}_\ell\varepsilon_\ell), \tag{3.43a}$$

$$f\to f-\sum_{i,\vec{r}}(p_ie_i+\tilde{g}_ie_i),$$

where noise correlations are

$$\langle\tilde{g}_\ell(\vec{r},t)\tilde{g}_{\ell'}(\vec{r}',t')\rangle=2A'_\ell\overline{T}\delta_{\ell,\ell'}\delta_{\vec{r},\vec{r}'}\delta(t-t'),$$

$$\langle\tilde{g}_i(\vec{r},t)\tilde{g}_{i'}(\vec{r}',t')\rangle=2a'_i\overline{T}\delta_{i,i'}\delta_{\vec{r},\vec{r}'}\delta(t-t'), \tag{3.43b}$$

i.e., the bare noise is Markovian. Here $\overline{T}\equiv k_BT/E_0$, and E_0 is an OP elastic energy given in Appendix B. For small stress and noise, a simple use of the substitution (1.4), justified by a detailed analysis, yields effective OP stresses and noises,

$$p_\ell^{tot}=p_\ell+p_\ell^c,\quad \tilde{g}_\ell^{tot}=\tilde{g}_\ell+\tilde{g}_\ell^c, \tag{3.44a}$$

where

$$p_\ell^c=\sum_i p_iS_{i\ell},\quad \tilde{g}_\ell^c=\sum_i\tilde{g}_iS_{i\ell}, \tag{3.44b}$$

with constants $S_{i\ell}$ as in Eqs. (3.24) and (3.34), respectively, for the TR and SR cases. The total correlations are

$$\langle\tilde{g}_\ell^{tot}(\hat{k},t)\tilde{g}^{*tot}_{\ell'}(\hat{k}',t')\rangle=2\overline{T}A'_{\ell,\ell'}(\hat{k})\delta_{\vec{k},\vec{k}'}\delta(t-t'), \tag{3.44c}$$

whereas in Eq. (3.28d),

$$A'_{\ell,\ell'}(\hat{k})\equiv\delta_{\ell,\ell'}A'_\ell+\sum_i a'_iS_{i\ell}S^*_{i\ell'}. \tag{3.44d}$$

The elimination of non-OP strains thus induces cross couplings, so non-OP stresses induce OP variations; noise correlations become spatially nonlocal; and different OP's acquire cross-correlated noises. The BG deterministic dynamics then becomes the BG Langevin dynamics of Eq. (1.3). For the TR case the noise is delta correlated in time. For the SR case with OP only, there is frequency dependence, but this can be circumvented by considering $\{\varepsilon_2,e_3\}$ of Eq. (3.32) as our system. Thus in both cases we have two variables with Markovian noises.

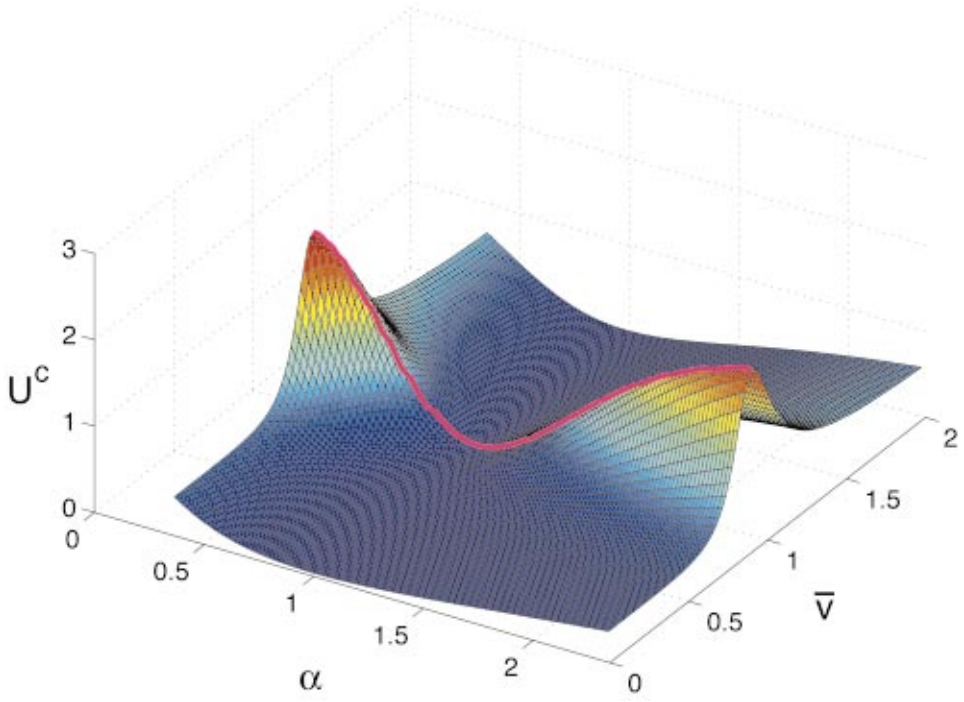

FIG. 2. (Color) Compatibility potential $U^c[\hat{k},\omega^2,(\omega/k)^2]$ for the square-rectangle SR case versus scaled velocity, $\overline{v}\equiv(4\rho_0/a_3)^{1/2}(\omega/k)$, and direction parameter $\alpha=k_x/k_y$ for frequency/dissipation parameter $\overline{\omega^2}=(\omega a'/a)^2=0.1$. Thus U^c is a repulsive and dynamic orientational potential, favoring diagonal textures, and moving interfaces.

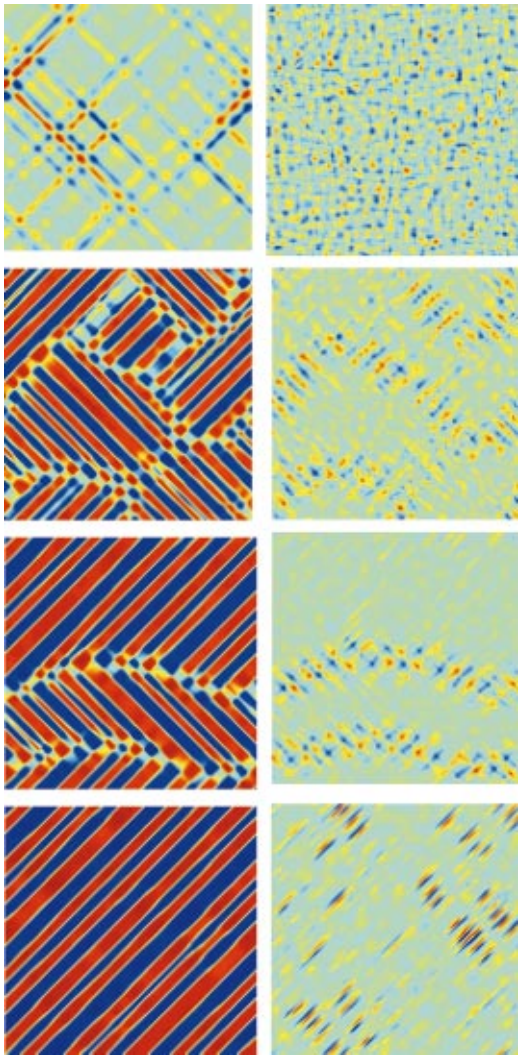

FIG. 3. (Color) Square-rectangle (SR) case: grain-boundary motion under BG-type dynamics. The columns show (top to bottom) temporal sequences for time t of 10, 20, 42, and 70 ps (see Appendix B). The initial conditions are $\varepsilon_2(\vec{r},t=0), e_3(\vec{r},t=0)$ random around zero mean. Parameters (defined in Appendix B) are $\rho_0=1, \tau=-0.25$, and the material is "hard," $a_1=100, a_3=210$; with $A_2'=1, a_3'=0.1=a_1'$. The time step is $\Delta t=10^{-4}$. Left column: the OP deviatoric strain $\varepsilon_2(\vec{r},t)$ under BG-equivalent dynamics (3.32), showing formation of twinlike regions separated by grain boundaries that are pushed out by domain-wall tip growth. Right column: non-OP shear strain $e_3(\vec{r},t)$, which is expelled from diagonal-domain regions, and concentrated in the pushed-out grain boundary regions (e_1 not shown). Diagnostics (Ref. 39) at $t=70$ were $E=-1.08, \langle\varepsilon_2\rangle=0.0012$, max-min $\varepsilon_2=(1.33,-1.35)$; max-min $e_3=(0.062,-0.058)$.

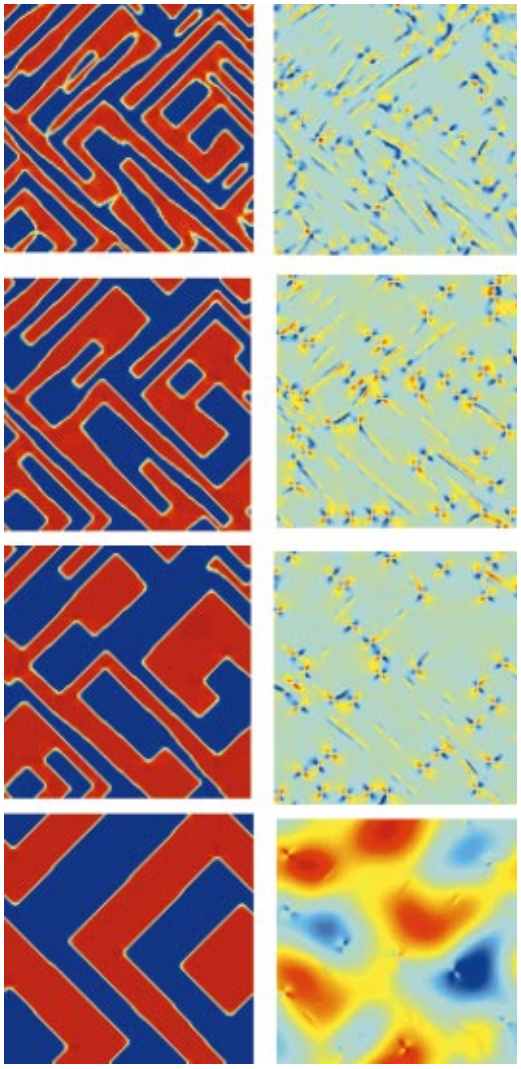

FIG. 4. (Color) Square-rectangle (SR) case: interface propagation under BG-type dynamics. The columns show (top to bottom) temporal sequences for time t of 40, 80, 160, and 1000 ps. The initial conditions are $\varepsilon_2(\vec{r},t=0), e_3(\vec{r},t=0)$ random around zero mean. Parameters (defined in Appendix B) are $\rho_0=1, \tau=-0.25$, and the material is "soft," $a_1=10, a_3=21$; with $A_2'=1=a_3', a_1'=0$. The time step is $\Delta t=0.002$. Left column: the OP deviatoric strain $\varepsilon_2(\vec{r},t)$ under BG dynamics (3.32), showing domain walls propagating under the repulsive long-range compatibility potential, giving the impression of a "zoom lens" moving in. Right column: non-OP shear strain $e_3(\vec{r},t)$, propagating outwards with interfaces, concentrated at corners (e_1 not shown). Diagnostics (Ref. 39) at $t=1000$ were $E=-1.4, \langle\varepsilon_2\rangle=0.0044$, max-min $\varepsilon_2=(1.23,-1.23)$; max-min $e_3=(0.33,-0.49)$.

D. Fokker-Planck description

Langevin dynamics with delta-correlated Markovian noise can be[46] equivalently written in a Fokker-Planck (FP) description. The set of $4L_0^2$ random variables labeled by $\alpha=\{\ell,\vec{k}\}$ is taken to be

$$\{x_\alpha\}=\{\varepsilon_2(\vec{k},t),\varepsilon_3(\vec{k},t)\},\quad \{v_\alpha\}=\{\dot{\varepsilon}_2(\vec{k},t),\dot{\varepsilon}_3(\vec{k},t)\}. \tag{3.45}$$

for the TR case, with $\varepsilon_3\to e_3$ for the SR case. The Langevin equations are

$$\dot{x}_\alpha(t)=v_\alpha(t),$$

$$\dot{v}_\alpha(t)=D_\alpha^{(1)}+\hat{\Gamma}_\alpha(t), \tag{3.46a}$$

where the frictional force plus internal stress, or "drift" term is

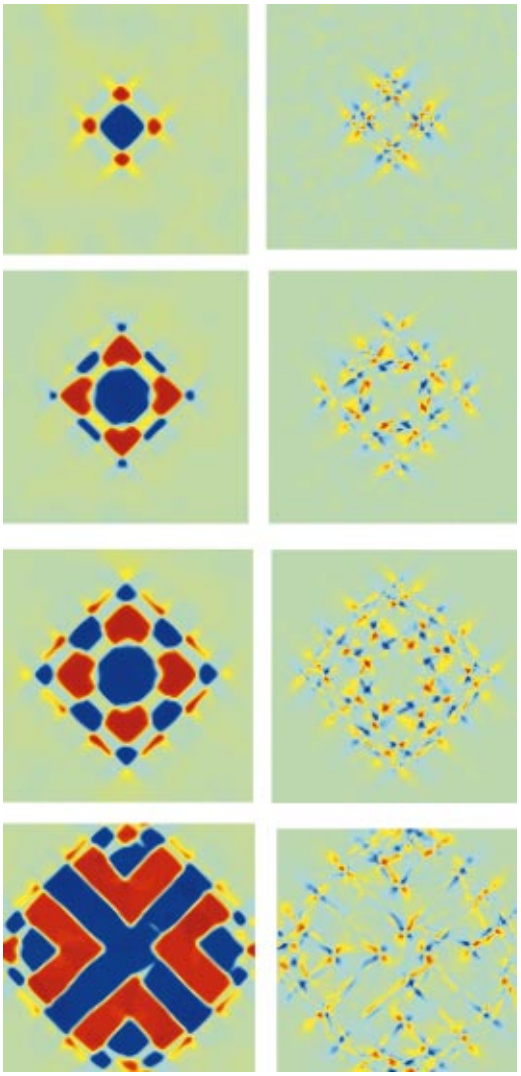

FIG. 5. (Color) SR case: strain evolution under BG-type dynamics, with a fixed, time-independent, Lorentzian-profile local stress. The sequence (top to bottom), for time $t=40$, 60, 76, and 106 ps with the same parameters as Fig. 3, but now $\tau=0.85$. Left column: dynamic texturing of deviatoric strain $\varepsilon_2(\vec{r},t)$. The system reduces the energy from the imposed single-sign strain by "elastic photocopying," or adaptive screening of the long-range elastic interaction, generating higher multipoles that propagate here. Right column: the non-OP shear strain $e_3(\vec{r},t)$ follows the OP propagation.

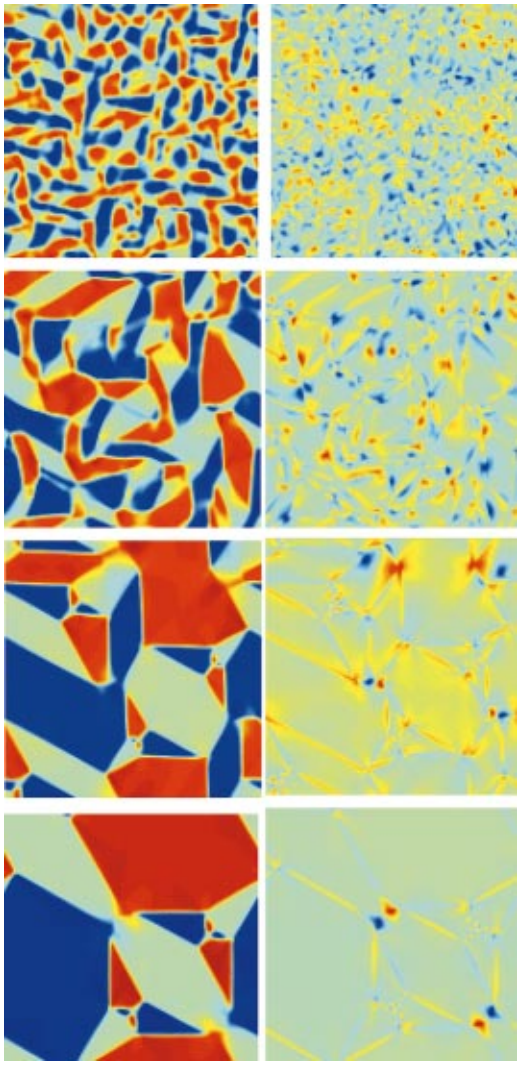

FIG. 6. (Color) Triangular to centered rectangle (TR) case: nested strain texturing under BG dynamics of Eq. (3.26). The columns show temporal sequences, with time t of 10, 40, 250, and 620 ps. The initial conditions for the OP strains are $\varepsilon_2(\vec{r},t=0),\varepsilon_3(\vec{r},t=0)$ random around zero mean. Parameters (defined in text) are $\rho_0=1$, $\tau=-50$, $a_1=1000$, $a_3=2100$; $A_2'=1$, $a_3'=1$, $a_1'=0$ and the time step is $\Delta t=10^{-3}$. Left column: the OP shear strain $\varepsilon_3(\vec{r},t)$ showing formation of nested star and triangle domains. Right column: non-OP compression strain $e_1(\vec{r},t)$, concentrated near domain corners, and expelled elsewhere. Diagnostics (Ref. 39) at $t=620$ were $E=-43.2$, $\langle\varepsilon_2\rangle=-0.003\,16$, $\langle\varepsilon_3\rangle=-1.05\times10^{-5}$, max-min $\varepsilon_2=(4.45,-2.62)$, max-min $\varepsilon_3=(3.63,-3.65)$.

$$D_\alpha^{(1)}=-\frac{1}{M(k)}\frac{\partial(F+F^c)}{\partial x_\alpha^*}-\sum_{\alpha'}D_{\alpha,\alpha'}^{(2)}v_{\alpha'}, \quad (3.46b)$$

where $M(k)=4\rho_0/k^2$ is a strain mass. The Langevin noise correlation is

$$\langle\hat{\Gamma}_\alpha(t)\hat{\Gamma}_{\alpha'}(t')\rangle=2D_{\alpha,\alpha'}^{(2)}\delta(t-t'), \quad (3.46c)$$

with "diffusion coefficient"

$$D_{\alpha,\alpha'}^{(2)}=\delta_{\vec{k},\vec{k}'}\overline{T}A'_{\ell,\ell'}(\hat{k})/M(k)^2. \quad (3.46d)$$

The FP equation in Kramers form[46] for the time-dependent probability $P(\{x_\alpha\},\{v_\alpha\},t)$ is

$$\partial P/\partial t=\hat{L}P\equiv[\hat{L}^{(1)}+\hat{L}^{(2)}]P, \quad (3.47a)$$

where the Fokker-Planck operator for ferroelastics is a sum of drift and diffusion terms, respectively, given by

$$\hat{L}^{(1)}=-v_\alpha\frac{\partial}{\partial x_\alpha^*}-\frac{\partial}{\partial x_\alpha^*}D_\alpha^{(1)},$$

$$\hat{L}^{(2)}=\sum_{\alpha,\alpha'}\frac{\partial^2}{\partial x^*_\alpha \partial x^*_{\alpha'}}D^{(2)}_{\alpha,\alpha'}. \tag{3.47b}$$

A formal solution for the probability in terms of the initial distribution is[46]

$$P(\{x_\alpha\},\{v_\alpha\},t)=e^{t\hat{L}}P(\{x_\alpha\},\{v_\alpha\},0). \tag{3.48}$$

The FP operator carries the nonlinearity, symmetries, anisotropies, and long-range spatial correlations. Its eigenvalues and eigenfunctions can be used to describe dynamic correlations. Since "potential conditions" hold,[46] the asymptotic probability is a Boltzmann distribution, which (as can be checked by substitution) is $P_0=\exp\{-[(F+F^c)+\frac{1}{2}\Sigma_\alpha M v_\alpha^2]/\overline{T}\}$. The free-energy minima thus correspond to probability peaks in OP function space, highest for zero strain rate. For uniform OP this implies a triple-well free energy, but for nonuniform textures there will be a more complex free-energy landscape. The multiple extrema are the TDGL asymptotic states.

The FP formalism is convenient for discussing textural dynamics, metastability, and glassy behavior; e.g., to determine strain correlations that correspond to experimentally probed response functions,[14,25] or to calculate temperature-dependent transformation rates through first-passage times.[15] Both strains and strain rates appear naturally, as in phenomenological models of elasticity and plasticity,[47] which could thereby be given a microscopic basis.

IV. BG DYNAMICS AS AN INHOMOGENEOUS ARRAY OF DAMPED AND COUPLED NONLINEAR OSCILLATORS

Here, we consider a mechanical analog of nonidentical damped oscillators, which suggests a physical scenario for nucleation and growth after a temperature quench. We first review well-known damped oscillator results, to fix notation and terminology, and regimes of validity.

A particle of mass M and friction parameter A, driven by a force $-F'\equiv-\partial F/\partial x=-Ax$ of spring constant $A\equiv F''$, obeys the underdamped equation

$$M\ddot{x}+A'\dot{x}=-F', \tag{4.1a}$$

which can be written in an equivalent convenient form

$$\ddot{x}=-(1/M)[\partial F/\partial x+A'\dot{x}], \tag{4.1b}$$

and the general solution is oscillations of exponentially decreasing amplitude. With natural frequency $\omega_0^2=F''/M$ and relaxation rate $\tau_0^{-1}\equiv A'/M$, the complex frequency is[48]

$$\omega'=\sqrt{\omega_0^2-(\tau_0)^{-2}}-i\frac{1}{2}\tau_0^{-1}. \tag{4.1c}$$

Thus, there is exponential decay (without even one complete oscillation) in the overdamped parameter limit of

$$\tau_0\omega_0<1, \tag{4.2}$$

when the inertial term is small at all times, and

$$\dot{x}(t)\approx-\lambda[\partial F/\partial x(t)], \tag{4.3a}$$

where $\lambda=1/A'$ describes the damped behavior. Outside this regime, it approximately describes the exponentially decaying envelope of the oscillations, at low frequencies/long times,

$$\omega\ll A'/M,\qquad t\gg 2\pi M/A'. \tag{4.3b}$$

Note that from Eq. (4.1c), and (4.3b), larger frequency/smaller mass oscillations are damped out earlier.

We now turn to BG-type evolution equations that cannot be obtained by adding simple local inertial terms to the standard overdamped dynamics such as Model *A* or *B* dynamics for a nonconserved or conserved order parameter, respectively.[49] However, defining an inverse mass $1/M(k)=1/\rho(k)=k^2/4\rho_0\sim k^2$ the apparently unusual BG structure of Eq. (3.26) for the TR case, say, can be written as

$$\ddot{\varepsilon}_\ell(\vec{k},t)=-[1/M(k)][\partial(F+F^c)/\partial\varepsilon^*_\ell(\vec{k},t)+A'_\ell\dot{\varepsilon}_\ell(\vec{k},t)], \tag{4.4a}$$

where, for simplicity, $a'_1=0$. On comparing with Eq. (4.1b), the dynamics has an intuitively appealing interpretation. It is the dynamics of a set of (nonlinear, coupled) oscillators, of (two-component) spring extension[50] $\varepsilon_\ell(\vec{k},t)$, labeled by k, with different masses $M(k)\sim 1/k^2$ that are strongly dependent on the oscillator label k: heaviest near the origin, and lightest at the (BZ) edge. Similarly, the damping rate $\tau_0(k)^{-1}\equiv A'/M(k)\sim k^2$ is smaller for the larger masses. The spring coupling $U^c(\hat{k})$ acts equally over all the BZ oscillators, in a given direction $\hat{k}$. Note that there is an intrinsically large range of damping times $\tau_0\sim k^{-2}$, over orders of magnitude. (This is reminiscent of decay times at criticality at a second-order critical point). From Eq. (4.4a) the $k\to 0$ infinite-mass oscillator is a special case, with its initial velocity $\dot{\varepsilon}(k\to 0,0)$ unchanged.[51]

Linearizing around equilibrium extensions, with effective curvature $F''=F''_0+K_0k^2\equiv A(k)$, and with $\omega_0^2\equiv A(k)/M(k)$, the complex frequency is

$$\omega'=\sqrt{\omega_0(k)^2-[\tau_0(k)]^{-2}}-i\frac{1}{2}\tau_0(k)^{-1}. \tag{4.4b}$$

The top panel of Fig. 7 shows that the angularly averaged strain structure factor $\overline{S(k,t)}=\langle|\varepsilon_2(\vec{k},t)|^2\rangle_{\delta k}$ or squared oscillator extension averaged over a shell $2\delta k$, is underdamped for small-k oscillators, but is overdamped for larger-k oscillators. The bottom panel shows asymptotic agreement between BG and TDGL dynamics. (See also Figs. 6 and 8). The initial strains are nonzero only in a 5×5 square region, and the oscillating strains show up as oscillating colors (not shown). The bottom panel shows that for the SR case the moment $\langle k^2\rangle$ takes on asymptotically the same value in the BG and TDGL dynamics.

From Eq. (4.4b), the long-wavelength modes are of necessity underdamped, with $\omega_0\tau_0\sim 1/k\gg 1$, a point made by Reid and Gooding.[6] We will, for simplicity, consider the regime where *none* of the oscillators are in the overdamped regime

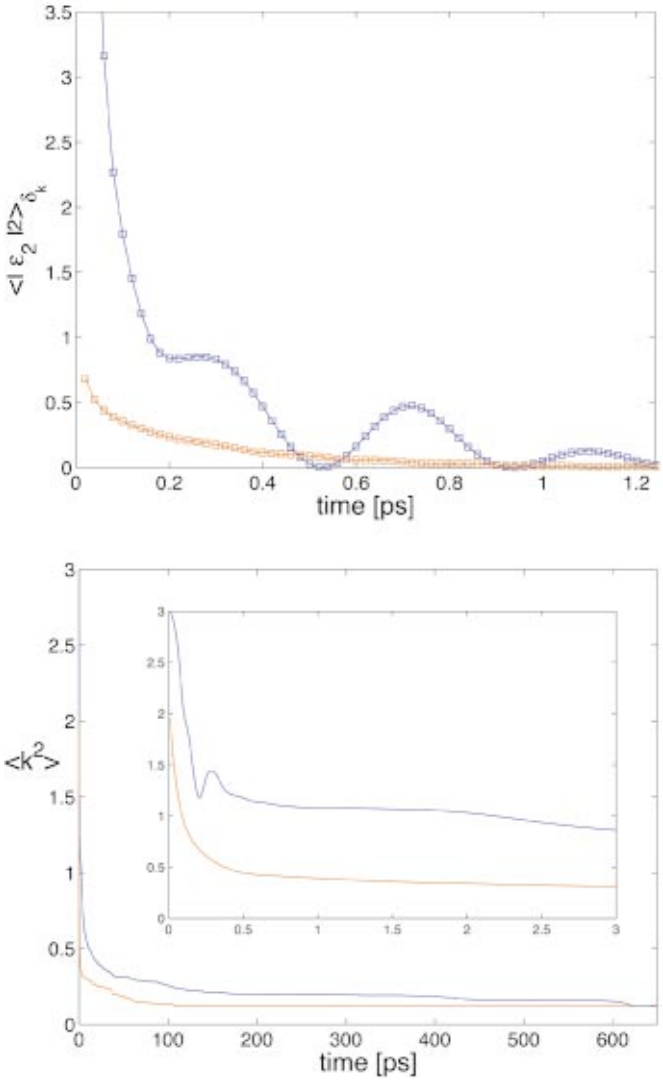

FIG. 7. (Color) Top: angularly averaged square oscillator extension or strain structure factor $\overline{S}(k,t)$ (defined in the text) versus time in picoseconds; for SR-case nonlinear BG-dynamics oscillators, labeled by k. The oscillators are at high temperatures $\tau=4$ (where there is only a single-well free energy), with parameters as in Fig. 4, and an initial condition as in text. The set of inhomogeneous strain oscillators of different mass $\sim k^{-2}$ and damping $\sim k^2$, are averaged over a shell of thickness $2\delta k$ in the Brillouin zone. The heavier, less damped oscillators with smaller $k=0.525$ (blue) oscillate, while the lighter, strongly damped oscillators with $k=2.65$ (red) are overdamped. The shells are $2\delta=0.05$ and 0.1, respectively. Bottom: comparison of $\langle k^2\rangle=\Sigma_k k^2|\varepsilon_3|^2/\Sigma_k|\varepsilon_3|^2$ for BG and TDGL dynamics for TR oscillators. The BG line (blue) asymptotically merges with the TDGL line (red). Inset shows early time damped oscillations in the BG case and overdamped monotonic decay for the TDGL case.

(4.2), i.e., $\tau_0(k)\omega_0(k)\gg 1$ for all k, even those at the BZ corner $k=\sqrt{2}\pi$. The oscillating, damped texture has to settle down to *some* time-independent state, which from Sec. III D will be a peak of the probability distribution, where the free-energy derivative is zero. Then an ''envelope dynamics'' as in Eq. (4.3a) for the OP strain is

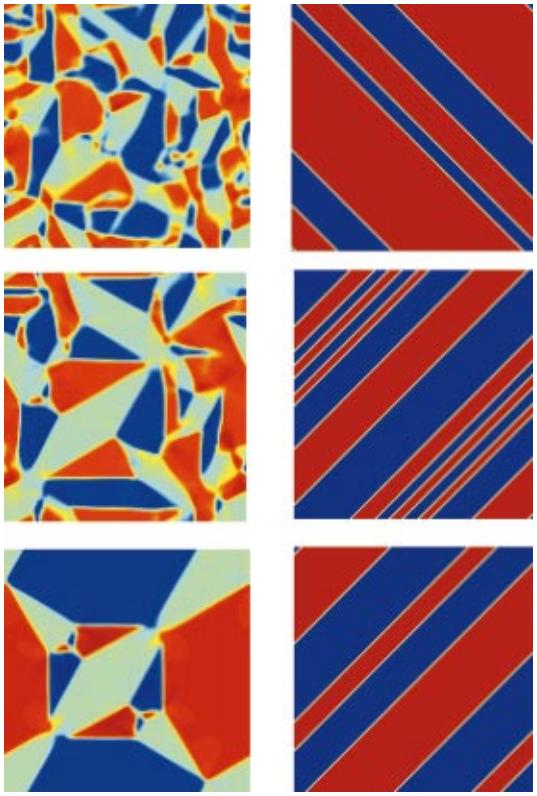

FIG. 8. (Color) Ordinary TDGL dynamics and OP textures. Left column: evolution for TR case with time $t=1$, 20, and 150 ps and parameters $a_1=1000,\tau=-50,A_2'=A_3'=1$. Right column: SR case, $a_1=100,a_3=210,\tau=-0.25,A_2'=1$ showing states evolved from different initial conditions, but the same parameters, illustrating nearly degenerate multiple free energy minima discussed in the text.

$$\dot{\varepsilon}_\ell(\vec{k},t)=-\lambda\frac{\partial(F+F^c)}{\partial\varepsilon_\ell^*(\vec{k},t)}, \tag{4.5a}$$

where $\lambda=1/A_\ell'$. However, the different-mass/friction oscillators can reach this late-time behavior only at different times t_k. Thus for times and lengths introduced through $\omega\sim 2\pi/t, k\sim\pi/L$, there is a wave vector dependent time scale $t>t_k$ or a time-dependent length scale $L<L_D(t)$ for textures to achieve the late-time regime, namely,

$$\omega\ll A'/M(k),\qquad t>t_k\equiv 2\pi/[(A'/4\rho_0)k^2],$$
$$L<L_D(t)=(t/t_D)^{1/2},\qquad t_D\equiv(4\rho_0/\pi A')^{1/2}, \tag{4.5b}$$

where t_D is the time for relaxation across a unit cell.

Taking the idea of a late-time equilibration length $L_D(t)$ as more generally applicable to the nonlinear case, a tentative picture emerges. While damped harmonic oscillators have trivial and identical final states, an inhomogeneous set of nonlinear oscillators with long-range coupling can have $\vec{k}$-dependent inhomogeneous final states $\{\varepsilon(\vec{k},t\to\infty)\}=\{\overline{\varepsilon}(\vec{k})\}$. The oscillations begin around the average value (say, zero) of the initial states $\{\varepsilon(\vec{k},t=0)\}$, for times $t>t_D$ after a temperature quench. Because of the k-dependent inhomogeneous damping of Eq. (4.4a), the lightest masses near

the BZ corner, with labels $\pi > k > \pi/L_D(t) \equiv k_D(t)$ will be the first to feel the final state attractor and begin oscillations around the final rather than the initial state. As time proceeds, the boundary shifts, and the circle of $k < k_D(t)$ ''initial-state'' oscillators shrinks, while the number of $\sqrt{2}\pi > k > k_D(t)$ ''final-state'' oscillators increases. Finally, all except the very smallest-k oscillators are on an equilibration path, and the larger-k ones [corresponding to structures of time-dependent size $L_D(t)$] have already reached it. There is thus *sequential-scale equilibration*, from the edge of the BZ inwards. For the SR case,[38] the additional $L_p(t)$ propagation length enriches the scenario. The tentative scenario is consistent with what we have seen in our simulations for given parameters, although the nonlinear mode coupling could induce more complex relaxation pathways, in more general parameter regimes.

Thus *the unusual* BG *dynamics implies unusual elastic properties.* Since $\rho(\vec{k}) \sim 1/k^2$, long-wavelength strains are kinematically blocked from decaying too early, and the scale-dependent damping and equilibration process starts at small-scale textures oriented by compatibility potentials, and then spreads to larger length scales, with associated non-OP strain expulsion. Consequently, materials classes governed by BG dynamics can have rich spatial patterning, metastability and glassiness, hierarchical multiscale microstructure, and a complex nonequilibrium elastic response.

V. LATE-TIME–SMALL-SCALE LIMITS OF DYNAMICS

We now show (for all frictions a_i', A_ℓ' nonzero) that the underdamped TR and SR equations are approximated by TDGL-type equations. The validity of TDGL dynamics in *any* regime was recently questioned[16] and an alternative overdamped dynamics, obtained by dropping displacement-acceleration terms in Eq. (2.8) was proposed.[16,17] Appendix C shows they are equivalent.

TR case dynamics

For the TR case, the late-time equations, from dropping OP strain-acceleration terms in Eq. (3.26), are with Eq. (3.28c),

$$\sum_{\ell'} A_{\ell,\ell'}(\hat{k}) \dot{\bar{\varepsilon}}_\ell(\vec{k},t) = -\frac{\partial(F+F^c)}{\partial \bar{\varepsilon}^*_\ell(\vec{k},t)}. \tag{5.1}$$

This truncation is valid only for textures in a low-frequency large-wave-vector regime as in Eq. (4.5b). For $a_1' = 0$ Eq. (4.5a) follows, while for the general case, an inversion yields

$$\dot{\bar{\varepsilon}}_\ell(\vec{k},t) = -\sum_{\ell'} \lambda_{\ell\ell'}(\hat{k}) \frac{\partial(F+F^c)}{\partial \varepsilon^*_{\ell'}(\vec{k},t)}, \tag{5.2a}$$

where the Onsager coefficient matrix is, with $A_2' = A_3'$,

$$\underset{=}{\lambda} = \frac{-1}{\mathcal{W}} \begin{bmatrix} A_3' + a_1' Q_{3,1}^2 & -a_1' Q_{2,1} Q_{3,1} \\ -a_1' Q_{2,1} Q_{3,1} & A_2' + a_1' Q_{2,1}^2 \end{bmatrix}, \tag{5.2b}$$

with the determinant (actually isotropic for $A_2' = A_3'$)

$$\mathcal{W} = A_2' A_3' \left[1 + \left(\frac{a_1'}{A_3'} \right) Q_{3,1}^2 + \left(\frac{a_1'}{A_2'} \right) Q_{2,1}^2 \right]. \tag{5.2c}$$

Since diagonal elements, and the determinant, of the λ matrix are nonzero, Eq. (5.2) implies that asymptotic textures $\bar{\varepsilon}_\ell(\vec{k})$ are determined by the extrema of the total free energy, which locate stable and metastable textural minima, as in the FP discussion of Sec. III D,

$$\partial(F+F^c)/\partial \bar{\varepsilon}^*_\ell(\vec{k}) = 0. \tag{5.3}$$

In coordinate space,

$$\dot{\bar{\varepsilon}}_\ell(\vec{r},t) = -\sum_{\ell'} \sum_{\vec{r}'} \lambda_{\ell\ell'}(\vec{r}-\vec{r}') \frac{\partial(F+F^c)}{\partial \varepsilon_{\ell'}(\vec{r}',t)}. \tag{5.4}$$

This is a time-dependent Ginzburg-Landau equation, with Onsager coefficients that are anisotropic and spatially *nonlocal*. For negligible non-OP friction parameter ($a_1'/A_2' \to 0$), the Onsager coefficient matrix becomes both spatially independent and diagonal in OP labels, yielding an ''ordinary'' TDGL equation with a constant, isotropic, and uniform friction:

$$\dot{\varepsilon}_\ell(\vec{r},t) = -\frac{1}{A_\ell'} \frac{\partial(F+F^c)}{\partial \varepsilon_\ell(\vec{r},t)}, \tag{5.5}$$

but still anisotropic and nonlocal in the elastic forces.

SR case dynamics

For the SR case, from dropping OP inertial terms in Eq. (3.36) in $\vec{k},\omega$ space,

$$F_2 - i\omega[A_2' + a_1' \eta^c(\hat{k},\omega^2,v^2)]\varepsilon_2 + a_1 U^c(\hat{k},\omega^2,v^2)\varepsilon_2 = 0. \tag{5.6a}$$

This can be written as a generalized TDGL-type equation with *retarded* Onsager kernels $\lambda(\vec{r}-\vec{r}',t-t')$ in coordinate space,

$$\dot{\varepsilon}_2(\vec{r},t) = -\int_{-\infty}^{t} dt' \sum_{\vec{r}'} \lambda(\vec{r}-\vec{r}',t-t') \frac{\partial(F+F^c)}{\partial \varepsilon_2(\vec{r}',t')}. \tag{5.6b}$$

Since the general TDGL structure is a ''current'' proportional to a ''force,'' the Onsager coefficient $\lambda(\vec{k},\omega) \equiv 1/[A_2' + \eta^c(\hat{k},\omega^2,v^2)]$ is like a dynamic ''conductivity.'' We consider, however, the low frequency $\omega \to 0$, or asymptotic long-time limit, keeping the linear term in frequency, but neglecting the quadratic and higher-order $\omega^2, (\omega/k)^2$ frequency dependence in the kernels. The regime of validity is considered below. This yields an instantaneous nonlocal TDGL equation as in the TR case, Eq. (5.4), with a single $\ell = 2$ order parameter. In Fourier space, $F^c = (a/2)\Sigma_{\vec{k},t} U_0^c(\hat{k}) |\varepsilon_2(\vec{k},t)|^2$, where the retarded compatibil-

ity potential reduces to the static expression[10,24] of Eq. (3.41) and the Onsager coefficient $\lambda(\hat{k})$ is given by $\lambda(\hat{k}) \equiv 1/[A_2' + a_1' \eta^c(\hat{k},0,0)]$.

For non-OP friction $a_{1,3}'/a_{1,3} \to 0$, η^c vanishes, and we again recover an ordinary (local, instantaneous) TDGL equation as in Eq. (5.5) and $\ell = 2$ with compatibility forces remaining nonlocal. Thus the model used in previous work[10] is a specific limit of the exact dynamics.

In a regime similar to Eq. (4.5b) (with $d'^2 = \max\{[a_1' a_3'/a_1 a_3], [a_1'/a_1)^2]\}$, the non-OP inertial delay $(\rho_0/a_3)(\omega/k)^2$ and frictional retardation $\sim(\omega d')^2$ can be, respectively, neglected, yielding Eq. (5.5), for lengths $L < \min[L_D(t), L_p(t)]$, and times $t > t_f \equiv (2\pi d')^{1/2}$. These simple heuristic estimates may not, of course, be strictly quantitative, but capture the diffusive aspect of the late-time relaxation. Figure 8, left column, shows that the TDGL dynamics[52] for the TR case yields textures similar to the (longer-run) BG dynamics of Fig. 6.

We note that the free energy can have several metastable minima with different microstructure, but closeby free-energy densities. Thus the nested stars of Fig. 6, under perturbation, yield rhombohedral structures of slightly lower energy density[53] (which are also obtained directly with a different initial random-number seed). The multiple-minima picture also emerges in TDGL simulations for the SR case of Fig. 8 where different random-number seeds produce three SR case quasitwin textures, with diagonal domains of different number and separation.[54] Such quasitwins were previously obtained in a displacement picture by Monte Carlo simulation.[24] The total free energies in each case are extensive $\sim L_0^2$, while their energy differences behave as the length $\sim K_0 L_0$ of the diagonal domain walls (with compatibility cost from U^c vanishing): the free-energy density difference is then $\sim 1/L_0$. (A surface compatibility potential sets a domain-wall separation length scale[10] and would raise the degeneracy, favoring equal-width ''true'' twins.) The barrier between states with differing numbers of walls is the cost $\sim A_1 L_0$ of a fractional-length kink in the domain wall and the barrier crossing time $\sim e^{(A_1 L_0/T)}$.

Thus, in general, the ALR potential can produce a multiple-minima free-energy landscape, with nearly degenerate, differently textured states separated by large barriers. Initial conditions or intermediate-state dynamical scales can lock the system into one of the metastable states. The possibility of multiple minima is consistent with recent analyses of models of competing short- and long-range interactions.[55]

In general, the inclusion of noise in BG-Langevin simulations will enable the system to more easily find low-energy minima. We now turn to other symmetries, and give the dynamics for the four crystal systems of 2D ferroelastic transitions.

VI. OP STRAIN DYNAMICS FOR ALL 2D-SYMMETRY TRANSITIONS

Since the derivations above involved the generic strain mass tensor and the harmonic non-OP strains and did not involve the details of the anharmonic OP free energy, the BG dynamics structure will be the same for all types of 2D (and indeed, 3D) transitions. However, the nature of the non-OP strains determines the symmetry of the compatibility kernels.

In 2D there are $N=3$ strains (compressional, deviatoric, and shear) and one compatibility equation ($N_c = 1$). The distinct ferroelastic transformations (Fig. 1), order parameters, and all possible symmetry-allowed combinations of strains in the Landau free energy, were found by Hatch *et al.*[35] using the computer program ISOTROPY. These transformations fall into two classes determined by the nature and number of order parameters.

(A) For either a two-component OP or two one-component OP's ($N_{op}=2, n=1$), we have the TR case, the TO case, and the square to oblique (SO) case, respectively.

(B) For a one-component OP, ($N_{op}=1, n=2$), we have the SR case with deviatoric OP; the square to centered rectangle (SC) case with shear OP; and the rectangle to oblique (RO) case with shear OP.

In 2D group theoretical symmetry notation, the transformations in Fig. 1 are (a) $p4mm$ to $p2mm$, (b) $p2mm$ to $p2$, (c) $p4mm$ to $c2mm$, (d) $p6mm$ to $c2mm$, (e) $p6mm$ to $p2$, and (f) $p4mm$ to $p2$. The OP compatibility kernels are frequency independent (dependent) for case A (B).

A. One non-OP strain, two OP strains ($N_{op}=2, n=1$)

TR case, driven by combined deviatoric and shear strains $\varepsilon_2, \varepsilon_3$. This is studied in the text above. The TO case differs from the TR case only in that F_0 [Eq. (3.27a)] includes terms up to sixth order in OP strains.

SO case, driven by independent deviatoric ε_2 and shear strains, ε_3. For the SO case, there are two distinct OP's that drive the transition, and the OP free energy is[35]

$$F_0 = \frac{1}{2} \sum_{\vec{r}} A_2 \varepsilon_2^2 + B_2 \varepsilon_2^4 + A_3 \varepsilon_3^2 + B_3 \varepsilon_3^4, \tag{6.1}$$

where the constants are merely illustrative. However, the harmonic non-OP energy and thus the form of the dynamics and the kernels, are identical in both cases.

B. Two non-OP strains, one OP strain ($N_{op}=1, n=2$)

SR *driven by deviatoric strain*, ε_2. This is considered in detail in the text above.

SC *driven by shear strain*, ε_3 The OP free energy now is as in Eq. (3.38a), but is $F_0(\{\varepsilon_3\})$. The non-OP harmonic energy, $f = \frac{1}{2}\Sigma_r a_1 e_1^2 + a_2 e_2^2$, and the dissipation is $R^{tot} = [\frac{1}{2}\Sigma_r a_1' \dot{e}_1^2 + a_2' \dot{e}_2^2 + A_3' \dot{\varepsilon}_3^2]$. Thus the derivation carries over, with the interchange $2 \leftrightarrow 3$, and, in particular, the compatibility factors and symmetry constants interchanged, $Q_2 \leftrightarrow Q_3, c_2 \leftrightarrow c_3$ in the dynamical kernel of Eq. (3.40). The $\omega \to 0$ limit, analogous to Eq. (3.41), is the static result.

$$a_1 U_0^c(\hat{k}) = \frac{a_1 Q_{3,1}^2}{[1 + (a_1/a_2) Q_{2,1}^2]}. \tag{6.2}$$

This is zero for $k_x=0$ or for $k_y=0$, so domain walls are either vertical or horizontal, as can be confirmed in simulations. The dynamics for e_2, ε_3 are

$$\rho_0 \ddot{e}_2 = -\frac{c_2^2 \vec{k}^2}{4}[Q_{2,1}Q_{3,1}(a_1\varepsilon_3 + a_1'\dot{\varepsilon}_3) + (a_1 Q_{2,1}^2 + a_2)e_2 + (a_1' Q_{2,1}^2 + a_2')\dot{e}_2, \quad (6.3a)$$

$$\rho_0 \ddot{\varepsilon}_3 = -\frac{c_3^2 \vec{k}^2}{4}[Q_{2,1}Q_{3,1}(a_1 e_2 + a_1'\dot{e}_2) + (F_3 + a_1 Q_{3,1}^2 \varepsilon_3) + (A_3' + a_1' Q_{3,1}^2)\dot{\varepsilon}_3]. \quad (6.3b)$$

RO driven by shear strain, ε_3. In this case the symmetry-adapted strains are the strain tensor components themselves, that is, $e_+ = E_{xx}$, $e_- = E_{yy}$ and $\varepsilon_3 = E_{xy}$. The non-OP free energy is

$$f = \frac{1}{2}\sum_r \{a_+ e_+^2 + a_- e_-^2\},$$

and the Rayleigh dissipation is

$$R^{tot} = \frac{1}{2}\sum_r \{A_3'\dot{\varepsilon}_3^2 + a_+\dot{e}_+^2 + a_-\dot{e}_-^2\},$$

with $a_\pm$, $a_\pm'$ the non-OP elastic and friction coefficients, respectively. The compatibility condition is $Q_+ e_+ + Q_- e_- + Q_3\varepsilon_3 = 0$, where in Fourier space $Q_+ = -k_y^2$, $Q_- = k_x^2$, $Q_3 = 2k_x k_y$. The derivation carries through, and the static compatibility kernel

$$a_+ U_0^c(\hat{k}) = \frac{a_+ (Q_3/Q_+)^2}{\left[1 + \left(\frac{a_+}{a_-}\right)\left(\frac{Q_-}{Q_+}\right)^2\right]} \quad (6.4)$$

is as in Eq. (6.2) with the substitution $1 \to +$, $2 \to -$ for subscripts.

VII. SUMMARY AND DISCUSSION

There are two themes in this paper: first, a derivation of ferroelastic evolution equations for all 2D symmetries, and second, a demonstration of a strain-based (rather than a displacement-based) description of elastic phase transitions.

We have, derived the $D>1$ underdamped dynamics for ferroelastics in terms of the OP strains $\{\varepsilon_\ell\}$ alone, showing that the evolution equations are of a generalized Bales-Gooding form. The strain-based derivation yields a wave vector dependent strain mass $\sim 1/\vec{k}^2$, thus large-scale strains have greater inertia. The structure is that of an OP strain acceleration, $\ddot{\varepsilon}_\ell$, proportional to a Laplacian acting on the sum of an OP-only stress and an OP-only frictional force. The stress and friction are strain and strain-velocity derivatives, respectively, of the effective free energy $F(\{\varepsilon_\ell\}) + F^c(\{\varepsilon_\ell\})$ and effective Rayleigh dissipation $R(\{\dot{\varepsilon}_\ell\}) + R^c(\{\dot{\varepsilon}_\ell\})$. These contain, in addition to direct local OP contributions (F and R), additional anisotropic and long-range contributions (F^c and R^c) that emerge from eliminating the non-OP strains using St. Venant's compatibility conditions. The kernels are explicitly evaluated for all 2D symmetries. There are also compatibility-induced noise contributions, and this BG-Langevin dynamics of Eq. (1.3) or Eq. (3.46) is a central result. A Fokker-Planck equation (3.47) is obtained. The BG dynamics can be regarded as nonlinear, nonlocally coupled oscillators labeled by $\vec{k}$, with unequal masses $\sim 1/\vec{k}^2$, and dampings $\sim \vec{k}^2$. The textures are the set of final rest positions $\{\varepsilon_\ell(\vec{k}, t\to\infty)\}$, with large-$k$ oscillators (small-scale strain textures) equilibrating first. The late-time envelope dynamics that guides the damped oscillations to this equilibration is of the TDGL form. This analog suggested an appealing picture of sequential-scale evolution for post-quench nucleation and hierarchical growth, accounting for nonuniform textures.

We adopt the strain picture in simulations, with strains as the basic variables on sites of a reference lattice, driven by symmetry-allowed terms of the Ginzburg-Landau free energy, and by anisotropic, symmetry-specific, long-range compatibility forces. The free energies are in a standardized form, with dimensionless parameters related to experiment. Simulations show that the generalized ($D>1$) BG dynamics has rich texturing properties, including repulsive velocity-resonant compatibility potentials that can drive interfaces at speeds (nearly) equal to the speed of sound.

We now place our results in perspective with some of the other models that have earlier provided valuable insights. Baus and Lovett[30] invoked the 19th century work of St. Venant[28,29] on the compatibility condition for the strain tensor, in the context of surface tension in liquids. They considered strain as the basic variable in the argument, and noted it might be useful in elastic solids. We similiarly work in the strain picture, differing in this respect from previous[14,15,24] simulations that work with $\vec{u}$ gradients, i.e., in the displacement picture.

In an interesting and important paper, Kartha *et al.*[24] performed Monte Carlo simulations to find static textures. They used the SR free energy that is sixth power in the deviatoric strain order parameter and harmonic in the compressional and shear non-OP strains, and the simulations were in terms of the displacement, so effectively $V = V(\{\vec{u}\})$. Since striking textures, such as unequal-separation diagonal domain walls (and tweed) were obtained, they attempted to understand these $\vec{u}$ simulation textures by using compatibility[29,30] to eliminate non-OP strains in the free energy, plotting (static) compatibility potentials. However, these effective strain-strain correlations were not directly used in the simulations. Such explicit implementation of the compatibility forces was done in TDGL dynamics, where quasitwins, the elastic Meissner effect (expulsion of non-OP strains), and tweed were investigated.[10] Other TDGL simulations also used compatibility forces to investigate tweed alone.[12] (The tweed terms considered[10,12,24] were all different.)

Our work has the same Lagrange-Rayleigh starting point[5,26] as Refs. 16 and 17, which focus early on in their argument on an overdamped-displacement dynamics. We fol-

low a different path and derive an OP-only underdamped strain dynamics, finding it is of a generalized BG form; and that the late-time limit is a TDGL-type equation.

Our approach differs from an underdamped dynamics[14] for the SR case, which did not explicitly consider non-OP strains; and phenomenologically added a static anisotropic long-range potential between squares of strains to explain acoustic signals.[25] We derive the BG structure from a Lagrangian with both non-OP strains and compatibility constraints, and find a *retarded* anisotropic long-range force in terms of the OP strains themselves (and not their squares). Our dynamics in the TDGL limit also differs from a TDGL dynamics,[8,42] where strains have been eliminated in favor of morphological profile variables, $\eta_\alpha(r,t)$, with α labeling the structural variants. The static potentials between squares of the morphological variables were obtained from elastic fields due to inclusions.[27]

Our approach is in the spirit of the Landau description of phase transitions:[56] working with the order parameters as the basic and physically relevant variables, and focusing on the order-parameter symmetries (as encoded in the compatibility factors), as the source of ferroelastic static and dynamic texturing.

Further work could include a detailed understanding of 2D nucleation,[57] growth, and interfacial profiles; extensions to 3D symmetries such as cubic to tetragonal[11] ($N_{op}=2, n=4, N_c=6$); extensions to improper ferroelastics where strain acts as a secondary OP (Ref. 58); generalizations to include defects, in a broader ''strain elastodynamics'' framework; making contact with phenomenologies of plasticity; simulations and calculations of experimentally measurable strain correlations and nonlinear susceptibilities; and exploring a hierarchical scenario for shape memory.[41]

The symmetry-specific, compatibility-focused underdamped ferroelastic dynamics for the strain order parameter encode, in their very structure, the possibility of an evolutionary textural hierarchy in both space and time, and a tendency for interfaces to be driven at the speed of sound, explaining some of the fascinating but puzzling features of martensitic dynamics. The dynamical equations could be applied to a wide variety of textural evolutions that include improper ferroelastics, leading to a deeper understanding of many materials of technological interest such as ferroelectrics, magnetoelastics, colossal magnetoresistance manganites, superconducting cuprates, and shape memory materials.

ACKNOWLEDGMENTS

It is a pleasure to acknowledge stimulating discussions with Professor G.R. Barsch, Professor S. Franz, Professor Y.B. Gaididei, Professor D.M. Hatch, Professor K. Kawasaki, and Professor J.A. Krumhansl. T.L. is grateful to The University of Western Ontario (UWO) and NSERC of Canada for support. S.R.S. thanks The Centre for Chemical Physics at UWO for support and the Theoretical Division, LANL for hospitality. This work was supported by the U.S. Department of Energy.

APPENDIX A: SQUARE TO RECTANGLE TRANSITION DYNAMICS

We need to demonstrate explicitly that the same dynamics results whether displacements or strains are treated as the basic independent variables. We derive, in two self-contained subsections the (same) underdamped dynamics for the SR case, (a) by varying the displacement, and (b) by varying the strains subject to compatibility.

1. Variation of displacements

The $(n=2)$ non-OP strains are here the compressional (e_1) and shear strains (e_3), and the $N_{op}=1$ deviatoric strain (ε_2) is the OP,

$$\frac{e_1}{c_1}=\frac{1}{2}(\Delta_x u_x+\Delta_y u_y), \quad \frac{\varepsilon_2}{c_2}=\frac{1}{2}(\Delta_x u_x-\Delta_y u_y),$$

$$\frac{e_3}{c_3}=\frac{1}{2}(\Delta_x u_y+\Delta_y u_x), \tag{A1}$$

with the free energy $V=f+F$, where

$$f=\frac{1}{2}\sum_r (a_1 e_1^2+a_3 e_3^2). \tag{A2a}$$

The Rayleigh dissipation function is

$$R^{tot}=\frac{1}{2}\sum_r [a_1'\dot{e}_1^2+a_3'\dot{e}_3^2+A_2'\dot{\varepsilon}_2^2]. \tag{A2b}$$

From Eq. (A2) and varying with respect to $\vec{u}$ as in Eq. (2.1) and (2.2) ,

$$\rho_0\ddot{u}_x=\frac{1}{2}\{\Delta_x[f_1+R_1]+\Delta_y[f_3+R_3]+\Delta_x[G_2+R_2]\}, \tag{A3a}$$

$$\rho_0\ddot{u}_y=\frac{1}{2}\{\Delta_y[f_1+R_1]+\Delta_x[f_3+R_3]-\Delta_y[G_2+R_2]\}. \tag{A3b}$$

This is the result of Ref. 17, where

$$f_{1,3}\equiv c_{1,3}\frac{\partial f}{\partial e_{1,3}}, \quad G_2\equiv c_2\frac{\partial F}{\partial \varepsilon_2},$$

$$R_{1,3}\equiv c_{1,3}\frac{\partial R^{tot}}{\partial \dot{e}_{1,3}}, \quad R_2\equiv c_2\frac{\partial R^{tot}}{\partial \dot{\varepsilon}_2}. \tag{A3c}$$

The underdamped strain equations with $\vec{\Delta}^2\equiv\Delta_x^2+\Delta_y^2, \hat{D}^2\equiv\Delta_x^2-\Delta_y^2$, are

$$\rho_0\ddot{e}_1=\frac{c_1}{4}[\Delta^2(f_1+R_1)+2\Delta_x\Delta_y(f_3+R_3)+\hat{D}^2(G_2+R_2)], \tag{A4a}$$

$$\rho_0\ddot{\varepsilon}_2=\frac{c_2}{4}[\hat{D}^2(f_1+R_1)+\vec{\Delta}^2(G_2+R_2)], \tag{A4b}$$

$$\rho_0\ddot{e}_3=\frac{c_3}{4}[2\Delta_x\Delta_y(f_1+R_1)+\vec{\Delta}^2(f_3+R_3)]. \tag{A4c}$$

We also have the compatibility relation of Eq. (3.6),

$$\hat{Q}_1 e_1 + \hat{Q}_2 \varepsilon_2 + \hat{Q}_3 e_3 = 0, \tag{A5}$$

where $\hat{Q}_1 = \vec{\Delta}^2/c_1, \hat{Q}_2 = -\hat{D}^2/c_2, \hat{Q}_3 = -2\Delta_x\Delta_y/c_3$. By taking derivatives of Eq. (A4) we see that Eq. (A5) is identically satisfied. Thus we can take Eqs. (A4a), (A4c), and (A5) as the three equations to determine the three strains, since then two of the equations are linear. Fourier transforming these three equations, we obtain for $e_{1,3}(\vec{k},\omega), \varepsilon_2(\vec{k},\omega)$,

$$\rho_0\omega^2\varepsilon_2 = \frac{1}{4}[c_1c_2(k_x^2 - k_y^2)a_{1\omega}e_1 + c_2^2k^2(F_2 - i\omega A_2'\varepsilon_2)], \tag{A6a}$$

$$\rho_0\omega^2 e_3 = \frac{1}{4}[c_1c_3 2k_xk_y a_{1\omega}e_1 + c_3^2k^2 a_{3\omega}e_3], \tag{A6b}$$

$$Q_1 e_1 = -Q_3 e_3 - Q_2\varepsilon_2, \tag{A6c}$$

where $F_2 = \partial F/\partial\varepsilon_2^*(\vec{k},\omega)$, $a_{1\omega} \equiv a_1 - i\omega a_1'$, $a_{3\omega} \equiv a_3 - i\omega a_3'$, and $Q_1 = k^2/c_2, Q_2 = (k_x^2 - k_y^2)/c_2, Q_3 = 2k_xk_y/c_3$.

Defining $b_\omega \equiv [a_{3\omega} - \rho_0(2\omega/k)^2]/a_{1\omega}$ and $B_\omega \equiv 1 + b_\omega(Q_1/Q_3)^2$, we obtain

$$e_1(\vec{k},\omega) = (Q_1/Q_3)b_\omega e_3(\vec{k},\omega),$$

$$e_3(\vec{k},\omega) = -(Q_2/Q_3B_\omega)\varepsilon_2(\vec{k},\omega). \tag{A7}$$

Using Eq. (A6), and Eq. (A7),

$$\rho_0\omega^2\varepsilon_2 = \frac{c_2^2}{4}k^2[F_2 - i\omega A_2'\varepsilon_2 + a_{1\omega}(Q_2/Q_3)^2(b_\omega/B_\omega)\varepsilon_2]. \tag{A8}$$

The dynamics is written out in BG form and discussed at the end of Sec. III.

2. Variation in strain

By varying Eq. (3.1) with respect to $e_{1,3}(\vec{r},t), \varepsilon_2(\vec{r},t)$, we obtain $N + N_c = 3 + 1 = 4$ equations,

$$\rho_{22}\ddot{\varepsilon}_2 + \rho_{21}\ddot{e}_1 = -\frac{\delta F}{\delta\varepsilon_2^*} - Q_2\Lambda - A_2'\dot{\varepsilon}_2, \tag{A9a}$$

$$0 = -a_3 e_3 - a_3'\dot{e}_3 - Q_3\Lambda, \tag{A9b}$$

$$\{\rho_{11}\ddot{e}_1 + \rho_{12}\ddot{\varepsilon}_2\} = -a_1 e_1 - a_1'\dot{e}_1 - Q_1\Lambda - a_3'\dot{e}_3, \tag{A9c}$$

$$Q_1 e_1 + Q_3\varepsilon_3 = -Q_2\varepsilon_2. \tag{A9d}$$

In $(\vec{k},\omega)$ space for $e_{1,3}(\vec{k},\omega), \varepsilon_2(\vec{k},\omega)$ and with $a_{1\omega} \equiv a_1 - i\omega a_1, a_{3\omega} \equiv a_3 - i\omega a_3$, there is one nonlinear equation,

$$\omega^2\rho_{22}\varepsilon_2 + \omega^2\rho_{21}e_1 = \frac{\delta F}{\delta\varepsilon_2^*} + Q_2\Lambda - i\omega A_2'\varepsilon_2 \tag{A10}$$

and $n + N_c = 3$ linear equations

$$0 = -a_{3\omega}e_3 - Q_3\Lambda, \tag{A11a}$$

$$-\omega^2\left(\frac{\rho_0}{c_3^2c_1Q_3}\right)e_3 = -a_{1\omega}e_1 + Q_1\Lambda = 0, \tag{A11b}$$

$$Q_1 e_1 + Q_3 e_3 = -Q_2\varepsilon_2, \tag{A11c}$$

where we have used a relation as in Eq. (3.21). From Eq. (A11a) we have the Lagrange multiplier,

$$\Lambda(\vec{k},\omega) = -\frac{a_{3\omega}e_3}{Q_3}, \tag{A12}$$

and hence the non-OP strains in terms of each other, $e_1 = b_\omega(Q_1/Q_3)e_3$. Finally, in terms of the OP,

$$e_3 = -(Q_2/Q_3)\varepsilon_2/B_\omega, \tag{A13a}$$

where

$$b_\omega \equiv \frac{[a_{3\omega} - \rho_0(2\omega/k)^2]}{a_{1\omega}}, \quad B_\omega \equiv 1 + b_\omega(Q_1/Q_3)^2. \tag{A13b}$$

Then

$$\frac{4\rho_0\omega^2}{c_2^2k^2}\varepsilon_2 = [F_2 - i\omega A_2'\varepsilon_2 + W\varepsilon_2], \tag{A14a}$$

where

$$W \equiv \frac{4\rho_0\omega^2}{c_2^2k^2} - \omega^2\left[\rho_{22} - \frac{Q_1Q_2}{Q_3^2}\frac{b_\omega\rho_{21}}{B_\omega} + a_{3\omega}\frac{(Q_2/Q_3)^2}{B_\omega}\right]. \tag{A14b}$$

We use the definitions (3.12) of $\rho_{22} = \rho_{11} = (4\rho_0/c_3^2k^2)(c_1Q_1/c_3Q_3)^2$, $\rho_{21} = (4\rho_0/k^2c_3^2)(Q_1Q_2/Q_3^2)\rho_{12}$, and $(Q_1^2 - Q_2^2)/Q_3^2 = (c_3/c_2)^2 = 1/2$ to obtain

$$\rho_0\omega^2\varepsilon_2 = \frac{c_2^2}{4}k^2[F_2 - i\omega A_2'\varepsilon_2 + a_{1\omega}(Q_2/Q_3)^2(b_\omega/B_\omega)\varepsilon_2]. \tag{A15}$$

Comparing with Eq. (A8), we see that the same dynamics results, whether displacement or strain is regarded as the independent variable, with compatibility enforced in the latter case. The BG evolution equation is discussed at the end of Sec. III.

A useful intermediate equation, obtained by substituting e_1 in terms of e_3 into Eq. (A10) and using Eq. (A12) for the Lagrange multiplier, expresses the equations as a coupled set for the OP and non-OP shear. This dynamics is given in Eq. (3.32), and is entirely equivalent to the OP-only retarded equation of Eq. (A15).

APPENDIX B: SCALING OF FREE ENERGY

Here we generalize the free-energy scaling of Barsch and Krumhansl[32] to scale the *Lagrangian* such that the Landau free energy is in a standard polynomial form; all the parameters are dimensionless; strains are of order unity and times are scaled in a characteristic time unit.

The symmetric strain tensor is related to displacement derivatives through

$$\phi_{\mu\nu}=\frac{1}{2}\left[\left(\frac{\partial U_\mu(\vec{r})}{\partial x_\nu}+\frac{\partial U_\nu(\vec{r})}{\partial x_\mu}\right)+\sum_\rho \frac{\partial U_\rho}{\partial x_\mu}\frac{\partial U_\rho}{\partial x_\nu}\right] \quad \text{(B1)}$$

and we retain the ''geometric nonlinearity,'' showing when it is negligible later. The symmetry-adapted compressional (ϕ_1), deviatoric (ϕ_2), and shear (ϕ_3) strains are

$$\phi_1/c_1=\frac{1}{2}(\phi_{xx}+\phi_{yy}), \quad \phi_2/c_2=\frac{1}{2}(\phi_{xx}-\phi_{yy}),$$

$$\phi_3/c_3=\frac{1}{2}(\phi_{xy}+\phi_{yx}), \quad \text{(B2)}$$

where c_1,c_2,c_3 are symmetry-specific constants. The free energy depends on the order parameter through a Landau term, and has non-OP and gradient contributions,

$$F=F_{Landau}+F_{non}+F_{Grad}. \quad \text{(B3)}$$

The order-parameter Landau energy is

$$F_{Landau}=\int d^3r\left[\sum_\ell \frac{1}{2}B^{(2)}(T)\phi_\ell^2+F_{poly}\right], \quad \text{(B4a)}$$

where $B^{(2)}(T)=B_0(T-T_c)$ vanishes at a characteristic temperature T_c, and F_{poly} is a temperature-independent OP polynomial with powers higher than quadratic, which is different for the SR and TR cases. The non-OP contribution is

$$F_{non}=\frac{1}{2}\int d^3r\sum_i B_i\phi_i^2, \quad \text{(B4b)}$$

while the gradient term is

$$F_{Grad}=\int d^3r\sum_\ell \frac{1}{2}K[\vec{\nabla}\phi_\ell]^2. \quad \text{(B4c)}$$

We assume uniformity in the z direction, of thickness h, and pass over to a 2D reference lattice of lattice constant a_o (square or triangular for SR and TR cases). Derivatives are converted to discrete lattice differences, and displacements are scaled in a_o. Thus

$$\frac{\partial}{\partial x_\mu}\to\frac{1}{a_o}\Delta_\mu, \quad \int d^3r\to ha_o^2\sum_{\vec{r}}. \quad \text{(B5)}$$

We further scale strains in a typical value λ chosen for convenience later, so that a scaled strain tensor $E_{\mu\nu}$ is then defined through

$$\phi_{\mu\nu}=\lambda E_{\mu\nu}=\frac{\lambda}{2}\left[\{\Delta_\mu u_\nu+\Delta_\nu u_\mu\}+\lambda\sum_\rho \Delta_\mu u_\rho\Delta_\nu u_\rho\right], \quad \text{(B6)}$$

so $\nabla_\mu U_\nu\to\lambda\Delta_\mu u_\nu$, where $\vec{u}$ is a dimensionless scaled displacement.[59] The scaled OP and non-OP strains are

$$\phi_\ell=\lambda\varepsilon_\ell, \quad \phi_i=\lambda e_i. \quad \text{(B7)}$$

The free energy (B3) can be written in terms of these scaled strains as

$$F=F_0(\{\varepsilon_\ell\},\tau)+f(\{e_i\})+F_{grad}(\{\vec{\Delta}\varepsilon_\ell\}), \quad \text{(B8)}$$

where

$$F_{non}/E_0\equiv f=\frac{1}{2}\sum_{\vec{r},i} a_i e_i^2, \quad \text{(B9a)}$$

$$F_{Grad}/E_0\equiv F_{grad}=\sum_{\vec{r},\ell}\frac{K_0}{2}(\vec{\Delta}\varepsilon_\ell)^2. \quad \text{(B9b)}$$

Here we multiply and divide by an energy density D_0 chosen later, to get the overall energy scale $E_0=ha_0^2D_0$ (this drops out in the end). The scaled parameters are

$$a_i=\frac{B_i\lambda^2}{D_0}, \quad K_0=\frac{K\lambda^2}{(a_o^2D_0)}. \quad \text{(B10)}$$

The scaled OP free energy is

$$F_{Landau}/E_0\equiv F_0=\sum_{\vec{r},\ell}(\tau-1)\varepsilon_\ell^2+F_{00}, \quad \text{(B11a)}$$

where $F_{00}\equiv F_{poly}/E_0+\Sigma_{\vec{r},\ell}\varepsilon_\ell^2$. The scaled temperature τ contains a physical temperature T_0 that fixes where $\tau=1$,

$$\tau\equiv\frac{(T-T_c)}{(T_0-T_c)}, \quad \left(\frac{B_0\lambda^2}{D_0}\right)\equiv\frac{1}{(T_0-T_c)}. \quad \text{(B11b)}$$

We now consider the SR and TR symmetries separately.

SR case scaling

For the SR case, $N_{op}=1$, there is only the deviatoric strain, as ϕ_2 is the order parameter and the polynomial is

$$F_{poly}=\int d^3r[-B^{(4)}\phi_2^4+B^{(6)}\phi_2^6]. \quad \text{(B12)}$$

In scaled form, the term in Eq. (B11a) is

$$F_{00}=\sum_{\vec{r}}[\varepsilon_2^2-C_0\varepsilon_2^4+\varepsilon_2^6], \quad \text{(B13)}$$

where we have factored out an energy density $D_0=B^{(6)}\lambda^6$ so the coefficient of the sixth-order term is unity, and $C_0\equiv B^{(4)}\lambda^4/D_0$. Now we choose λ to fix C_0 so that for three ($\alpha=+,-,0$) roots $\bar{\varepsilon}_2^{\alpha}$ at $\tau=1$, the conditions of degeneracy

$$F_{00}(\{\bar{\varepsilon}_\ell^{(\alpha)}(1)\})=F_0(\{\bar{\varepsilon}_\ell^{(\alpha)}(1)\},\tau=1)=0, \quad \text{(B14)}$$

and normalization

$$\sum_\ell[\bar{\varepsilon}_\ell^{(\pm)}(1)]^2=1 \quad \text{(B15)}$$

are satisfied, and hence determine the typical strain λ and all scaled parameters. For the SR case,

$$C_0=2, \quad \lambda=(B^{(4)}/2B^{(6)})^{1/2}, \quad D_0=(B^{(4)}/2)^3/(B^{(6)})^2, \quad \text{(B16)}$$

with the C_0 "completing the square" in F_{00} and thus the OP free energy is

$$F_0=\sum_r\ (\tau-1)\varepsilon_2^2+\varepsilon_2^2(\varepsilon_2^2-1)^2. \tag{B17}$$

The $\tau=1$ roots, $\overline{\varepsilon_2^{(\pm)}}=\pm 1$, then manifestly satisfy the conditions (B14) and (B15).

To get an idea of parameters, we use FePd shape memory alloy values,[24] for the SR case with energy densities in units of ergs/cm^3, $B_1=1.4\times10^{12}$, $B_2=2.8\times10^{12}$, $C_2=1.7\times10^{12}$, $D_2=3\times10^{17}$, $K/a_o^2=2.5\times10^{11}$, and $B_o=2.4\times10^9$ ergs/cm^3 K. This gives, from Eq. (B6), the typical strain value $\lambda=0.02$, elastic constants $a_1=155\approx a_3/2$; OP variation scale $\sqrt{K_0}\approx5$, an elastic energy density $E_0/a_0^2h=D_0=3.8\times10^6$ ergs/cm^3, and a temperature separation $T_0-T_c=7$ K. (The magnitude of D_0 corresponds to a magnetic energy density $H^2/8\pi$ for fields ~1 T.) Note that $\lambda\ll1$, thus in Eq. (B6) we may drop the "geometric nonlinearity" and work with the linear Cauchy strain tensor, as in the text, that satisfies the simple St. Venant compatibility condition. External stresses (e.g., compressional) enter as $F\rightarrow F+\Sigma_r p_1 e_1$ with scaled pressure $p_1=1$ corresponding to $D_0/\lambda=0.02$ GPa.

Inertial and damping terms

Using the same kind of transformations, the dimensionless inertial (T) and damping (R^{tot}) contributions to the Lagrangian are

$$T=\frac{1}{2}\int d^3r\rho_m\left(\frac{\partial U}{\partial t}\right)^2\Big/\ E_o=\frac{1}{2}\sum_r\ \rho_0\dot{u}^2 \tag{B18a}$$

and

$$R^{tot}=\frac{1}{2}\int d^3r\sum_{j=1,2,3}B_j\left(\frac{\partial\phi_j}{\partial t}\right)^2\Big/\ E_0$$

$$=\frac{1}{2}\sum_r\ [a_1'\dot{e}_1^2+a_3'\dot{e}_3^2+A_2'\dot{\varepsilon}_2^2], \tag{B18b}$$

where the dots are dimensionless time derivatives, and we introduce a characteristic time unit t_o, with dimensionless density ρ_0 and friction coefficients $a_{1,3}'$ and A_2' defined as

$$\rho_0=\frac{\rho_m\lambda^2a_o^2}{t_o^2D_o},\quad \frac{a_{1,3}'}{a_{1,3}}=\frac{B_{1,3}'}{B_{1,3}t_o^2},\quad A_2'=\frac{B_2'/B_ot_o^2}{(T_o-T_c)}. \tag{B19}$$

Here we have used Eqs. (B10) and (B11b) for $a_{1,3}$ and (T_o-T_c). Wave propagation crossing a nanometer in a picosecond corresponds to a sound speed of 1000 m/s. We take t_o to be of the order of inverse phonon frequencies and the scaled friction coefficients $a_{1,3}',A_2'$ are then less than unity. With a mass density of $\rho_m=10$ g/cm^3, lattice constant $a_o\sim3$ Å, and $t_o\sim10^{-12}$ s the dimensionless density, or ratio of kinetic and elastic energy densities is $\rho_0\sim1$. We work with parameters $\rho_0=1,K_0=1,t_0=1$ picosecond, a fixed ratio $a_3/a_1=2.1$, and $a_1=100$ or 10, with a_1',A_2',a_3' as unity or less.

TR case scaling

For the TR case we start from[6,16] a free-energy density in $F_{poly}\sim-B^{(3)}(\phi_2^3-3\phi_2\phi_3^2)+B^{(4)}(\phi_2^2+\phi_3^2)^4$. We follow the same procedure as above: (i) scaling strains as in Eq. (B7); (ii) pulling out a common factor $D_0\equiv B^{(4)}\lambda^4$; (iii) choosing λ in $C_0\equiv B^{(3)}\lambda^3/D_0$ to satisfy Eq. (B15). This gives

$$C_0=2,\quad \lambda=B^{(3)}/2B^{(4)},\quad D_0=(B^{(3)}/2)^4/(B^{(4)})^3. \tag{B20}$$

The scaled free energy is then

$$F_{00}=\sum_{\vec{r}}\ (\varepsilon_2^2+\varepsilon_3^2)-2(\varepsilon_2^3-3\varepsilon_2\varepsilon_3^2)+(\varepsilon_2^2+\varepsilon_3^2)^2 \tag{B21a}$$

$$=\sum_{\vec{r}}\ 3(1+2\varepsilon_2)\left[\varepsilon_3^2-\frac{1}{3}(1-\varepsilon_2^2)\right]+[\varepsilon_2^2+\varepsilon_3^2-1]^2. \tag{B21b}$$

Here the second form explicitly displays the (B14),(B15) conditions, for $\tau=1$, when the roots are $(\varepsilon_2^{(0)},\varepsilon_3^{(0)})=(1,0)$; $(\varepsilon_2^{(\pm)},\varepsilon_3^{(\pm)})=(-\frac{1}{2},\pm\sqrt{3}/2)$, and lie on a unit circle.

Connection to other scalings

The SR free energy of Ref. 17 can be written as our Eqs. (B9), (B17), and (B18b) by a scaling of strains in $\alpha=10^6$, giving an overall factor $\frac{1}{2}\alpha^2$ absorbed in the TDGL time. (The elastic and frictional constants are then half our a_i,a_i' .) A similiar TR scaling in $\alpha=10^3$ yields our Eq. (B21), with a common factor of $\frac{1}{2}$ relating elastic/friction constants.[16] Similar scaling can be performed for other symmetries.

APPENDIX C: TRUNCATED DISPLACEMENT DYNAMICS AND TDGL EQUATIONS

We have shown that the BG equations, dropping strain accelerations in an ω vs k regime, yield TDGL equations. On the other hand, dropping *displacement* accelerations in Eq. (2.8) or Eq. (A3) yields equations stated to be different[16,17] from the TDGL form. In this appendix, we demonstrate their equivalence to TDGL.

More generally, the truncation is like dropping all the inertial terms in the Lagrange-Rayleigh equations (3.1) and (3.2),

$$\sum_\nu\ \partial_\nu\sigma_{\mu\nu}=-\sum_\nu\ \partial_\nu\sigma'_{\mu\nu}, \tag{C1}$$

given as a balance[17] between derivatives of the stress tensor $\sigma_{\mu\nu}=\delta L/\delta E_{\mu\nu}$ and the damping force tensor $\sigma'_{\mu\nu}=\delta R^{tot}/\delta\dot{E}_{\mu\nu}$. Clearly,[17] one cannot proceed in two dimensions by simply dropping the ∂_ν derivatives in Eq. (C1). Such a procedure would give $\sigma_{\mu\nu}=-\sigma'_{\mu\nu}$, which is not

quite correct. For the SR transformation, for example, this is $\dot{e}_{1,3}=-(a_{1,3}/a'_{1,3})e_{1,3}$; and $\ddot{\varepsilon}_2=-(1/A'_2)(\partial F/\partial\varepsilon_2)$, where $F\sim\varepsilon_2^6$ is just the local triple-well free energy. This is the kind of overdamped dynamics,[7] without compatibility contributions, that would emerge if all the strains were independent.

We now show that the truncated displacement dynamics (C1) is in fact a TDGL dynamics.

TR case displacement truncations

Dropping $\{\ddot{u}_\mu\}$ and keeping $\Delta_\mu\dot{u}_\nu$ in Eq. (2.8) yields[16] equations that in Fourier space are

$$a'_1k_x\dot{e}_1+A'_2k_x\dot{\varepsilon}_2+A'_3k_y\dot{\varepsilon}_3=-\{a_1k_xe_1+k_xF_2+k_yF_3\}, \tag{C2a}$$

$$a'_1k_y\dot{e}_1-A'_2k_y\dot{\varepsilon}_2+A'_3k_x\dot{\varepsilon}_3=-\{a_1k_ye_1-k_yF_2+k_xF_3\}. \tag{C2b}$$

Using compatibility (3.18d) we can eliminate

$$e_1=-[Q_2(\vec{k})\varepsilon_2+Q_3(\vec{k})\varepsilon_3]/Q_1(\vec{k}), \tag{C3}$$

where $Q_2/Q_1=[(k_x^2-k_y^2)/k^2]$; $Q_3/Q_1=2k_xk_y/k^2$. Further, Eq. (C2) can be written in matrix form as

$$\underline{\underline{\mathbf{M}}}\begin{pmatrix}\dot{\varepsilon}_2\\ \dot{\varepsilon}_3\end{pmatrix}=-\begin{pmatrix}k_x & k_y\\ k_y & -k_x\end{pmatrix}\begin{pmatrix}F_2+F_2^c\\ F_3+F_3^c\end{pmatrix}, \tag{C4}$$

where $M_{\ell\ell'}$ is defined as $M_{22}=k_x[A'_2-a'_1Q_2/Q_1]$,$M_{33}=-k_x[A'_3-(k_y/k_x)a'_1(Q_3/Q_1)]$, $M_{23}=k_y[A'_3-a'_1(k_x/k_y)(Q_3/Q_1)]$, $M_{32}=k_y[A'_2+a'_1(Q_2/Q_1)]$. Here F_2^c,F_3^c are chosen to match the right-hand side terms of Eq. (C2), so that $F_2^c=a_1[(Q_2^2/Q_1^2)\varepsilon_2+(Q_2Q_3/Q_1^2)\varepsilon_3]$, and $F_3^c=a_1[(Q_2Q_3/Q_1^2)\varepsilon_2+a_1(Q_3/Q_1)^2\varepsilon_3]$ and can be written as derivatives of a compatibility potential F^c,

$$F_{2,3}+F_{2,3}^c=\frac{\partial(F+F^c)}{\partial\varepsilon^\star_{2,3}(\vec{k})}, \tag{C5}$$

where $F^c=\frac{1}{2}a_1\Sigma_{\vec{k}}U^c_{\ell\ell'}\varepsilon_\ell(\vec{k},t)\varepsilon^*_{\ell'}(\vec{k},t)$ with $U^c_{\ell\ell'}\equiv Q_\ell Q_{\ell'}/Q^2{}_1$. Inverting the matrix $\underline{\underline{\mathbf{M}}}$ of Eq. (C4) yields Eq. (5.2), and then the TDGL link is as in the text. For a choice[16] $a'_1=0$, one gets the ordinary (local, instantaneous) TDGL equation, namely, Eq. (5.5).

SR case displacement truncations

Similarly for the SR case, dropping displacement accelerations compared to gradients of displacement velocities[17] in Eq. (A3) yields the Fourier space equation, with $a_{i\omega}\equiv a_1-i\omega a'_i$,

$$\left(\frac{c_1}{c_2}\right)a_{1\omega}e_1+\left(\frac{c_3}{c_2}\right)a_{3\omega}\left(\frac{k_y}{k_x}\right)e_3=-[-i\omega A'_2+F_2], \tag{C6a}$$

$$\left(\frac{c_1}{c_2}\right)a_{1\omega}e_1+\left(\frac{c_3}{c_2}\right)a_{3\omega}\left(\frac{k_x}{k_y}\right)e_3=[-i\omega A'_2+F_2]. \tag{C6b}$$

Then compatibility $e_1+(Q_2/Q_1)\varepsilon_2+(Q_3/Q_1)e_3=0$ gives

$$e_1=\left(\frac{Q_1}{Q_3}\right)\left(\frac{a_{3\omega}}{a_{1\omega}}\right)e_3,$$

$$e_3=-\left[\frac{\left(\frac{Q_2}{Q_3}\right)}{1+\left(\frac{a_{3\omega}}{a_{1\omega}}\right)\left(\frac{Q_1}{Q_3}\right)^2}\right]\varepsilon_2. \tag{C7}$$

Hence

$$-i\omega A'_2\varepsilon_2=-F_2+\left[\frac{a_{3\omega}\left(\frac{Q_2}{Q_3}\right)^2}{1+\left(\frac{a_{3\omega}}{a_{1\omega}}\right)\left(\frac{Q_1}{Q_3}\right)^2}\right]\varepsilon_2. \tag{C8}$$

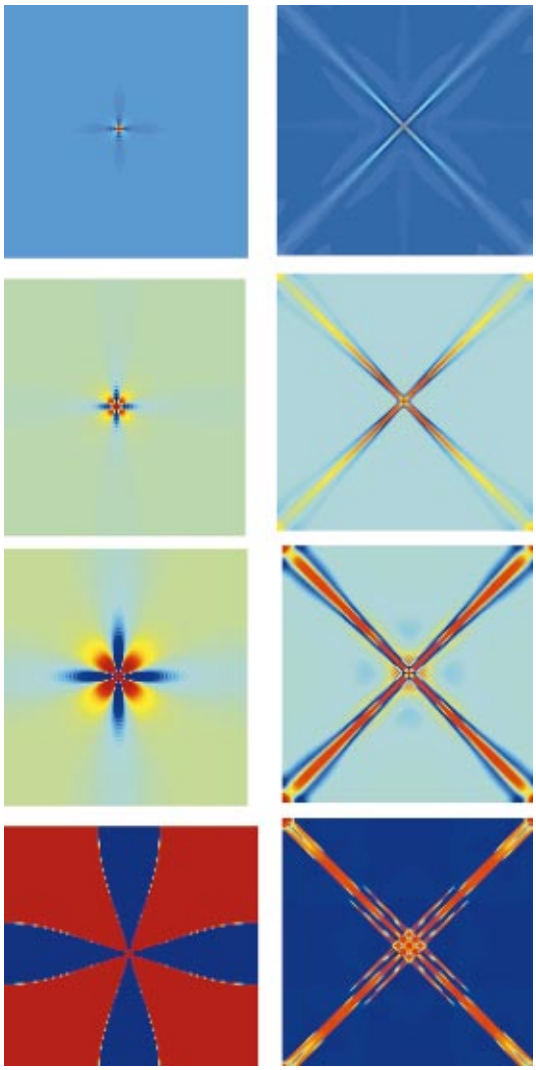

FIG. 9. (Color) Evolution from single-site initial condition for SR case under ordinary TDGL dynamics. Times are $t=0.13,0.16,0.18,\ 0.24$ ps, with $\Delta t=10^{-4}$. The initial condition is $\varepsilon_2(\vec{r},t=0)=0.0001$ at a single site and zero elsewhere. Non-OP friction constants are $a'_1=0=a'_3$. Left column: "soft" case, $a_1=2,a_3=2,\tau=-50,A'_2=2$. Right column: "hard" case, $a_1=2000,a_3=2000,\tau=-50,A'_2=2$. (Since colors are relative, the background changes, with changes in evolving average intensity.)

Separating real and imaginary parts of the square brackets, and using the notation of Eq. (3.35),

$$-i\omega\varepsilon_2 = -\lambda(\hat{k},\omega)[F_2 + a_1 U^c(\hat{k},\omega^2,0)\varepsilon_2], \qquad \text{(C9)}$$

where now $\lambda(\hat{k},\omega) = 1/[A_2' + a_1' \eta^c(\hat{k},\omega^2,0)]$. This is manifestly a generalized TDGL as in Eq. (5.6a), but with a partial truncation of the kernel, which drops the (resonant) inertial delay terms $(\rho_0/a_3)(\omega/k)^2$ and keeps only frictional retardation. It is thus valid for a narrowly restricted, intermediate length and time regime roughly estimated as $L_D(t) > L_p(t) > L$ and $t < t_f$ (see Sec. V). Taking a more well-defined limit of late times (dropping all ω^2) the static kernel $U^c(\hat{k},0,0)$ becomes a good approximation, and the nonlocal TDGL (5.4) with $\ell,\ell' = 2$ holds. For $a_{1,3}'/a_{1,3} \ll A_2'$ as for ''hard'' systems,[17] this collapses to a *local* TDGL, as in Eq. (5.5). Thus, overdamped displacement equations[16,17] are TDGL equations in disguise and not a new dynamics. As expected, simulation of TDGL equations produce the same textures[16,17] from similar initial conditions.

Figure 9 shows ordinary TDGL simulations with an initial condition[17] of strain nonzero at a single point and zero elsewhere. This is like a stress applied at a single point and then removed. Flowerlike or diagonal-cross textures similiar to Ref. 17 are obtained, for both ''soft'' and ''hard'' materials.

Reference 17 could not reproduce a TDGL structure given in Fig. 4(b) of Ref. 10, part of a multipanel figure that displays stress effects for soft materials. In the intermediate-temperature $(1 > \tau > 0)$ phase, Ref. 10 considered the effect of two Lorentzian deviatoric stresses, fixed and continuously maintained. The motivation was to see if a stress seed analogous to a seed crystal in a supercooled melt, could yield stress-induced martensitic twins even for positive $\tau = 0.3$. The Ref. 17 simulations did not have the applied constant stress of Ref. 10, and moreover, were at very low temperatures $\tau = -50$. We conclude that the difference in results is due to a difference in states investigated, and *not* a difference in dynamics, which is TDGL-like in both cases.

[1] V. K. Wadhawan, *Introduction to Ferroic Materials* (Gordon and Breach, Amsterdam, 2000).

[2] E. K. H. Salje, *Phase Transformations in Ferroelastic and Coelastic Solids* (Cambridge University Press, Cambridge, UK, 1990).

[3] Z. Nishiyama, *Martensitic Transformations* (Academic, New York, 1978).

[4] *Shape Memory Materials*, edited by K. Otsuka and C. M. Wayman (Cambridge University Press, Cambridge, UK, 1998).

[5] G.S. Bales and R.J. Gooding, Phys. Rev. Lett. **67**, 3412 (1991).

[6] A.C.E. Reid and R.J. Gooding, Phys. Rev. B **50**, 3588 (1994); Physica A **239**, 1 (1997); B.P. Van Zyl and R.J. Gooding, Metall. Mater. Trans. A **27A**, 1203 (1996).

[7] S.K. Chan, J. Chem. Phys. **67**, 5755 (1977).

[8] Y. Wang and A.G. Khachaturyan, Acta Mater. **45**, 759 (1997); S. Semenovskaya, Y.M. Zhu, M. Suenaga, and A.G. Khachaturyan, Phys. Rev. B **47**, 12 182 (1993); Y. Wang and A.G. Khachaturyan, Acta Mater. **45**, 759 (1997).

[9] W.C. Kerr, M.G. Killough, A. Saxena, P.J. Swart, and A.R. Bishop, Phase Transitions **69**, 247 (1999).

[10] S.R. Shenoy, T. Lookman, A. Saxena, and A.R. Bishop, Phys. Rev. B **60**, R12537 (1999).

[11] K.Ø. Rasmussen, T. Lookman, A. Saxena, A.R. Bishop, R.C. Albers, and S.R. Shenoy, Phys. Rev. Lett. **87**, 055704 (2001). The $N_c = 6$ compatibility equations are actually in two sets of three equations (see L.E. Malvern in Ref. 29).

[12] Y. Yamazaki, J. Phys. Soc. Jpn. **67**, 1587 (1998); **67**, 2970 (1998).

[13] A. Onuki, J. Phys. Soc. Jpn. **68**, 5 (1999).

[14] R. Ahluwalia and G. Ananthakrishna, Phys. Rev. Lett. **86**, 4076 (2001).

[15] M. Rao and S. Sengupta, Phys. Rev. Lett. **78**, 2168 (1997); cond-mat/0107098 (unpublished).

[16] S.H. Curnoe and A.E. Jacobs, Phys. Rev. B **63**, 094110 (2001).

[17] S.H. Curnoe and A.E. Jacobs, Phys. Rev. B **64**, 064101 (2001).

[18] J. A. Krumhansl, in *Lattice Effects in High-T_c Superconductors*, edited by Y. Bar-Yam, T. Egami, J. Mustre de Leon, and A. R. Bishop (World Scientific, Singapore, 1992).

[19] A. Asamitsu, Y. Moritomo, Y. Tomioka, Y. Arima, and Y. Tokura, Nature (London) **373**, 407 (1995).

[20] A. Moore, J. Graham, G.K. Williamson, and G.R. Raynor, Acta Metall. **3**, 579 (1955).

[21] G.R. Barsch, B. Horovitz, and J.A. Krumhansl, Phys. Rev. Lett. **59**, 1251 (1987); B. Horovitz, G.R. Barsch, and J.A. Krumhansl, Phys. Rev. B **43**, 1021 (1991).

[22] M. Sugiyama, Ph.D. thesis, Osaka University, 1985; S. Muto, R. Oshima, and F.E. Fujita, Acta Metall. Mater. **38**, 685 (1990).

[23] A. Saxena and G.R. Barsch, Physica D **66**, 195 (1993).

[24] S. Kartha, J.A. Krumhansl, J.P. Sethna, and L.K. Wickham, Phys. Rev. B **52**, 803 (1995).

[25] L. Carrillo, L. Mañosa, J. Ortin, A. Planes, and E. Vives, Phys. Rev. Lett. **81**, 1889 (1998).

[26] L. D. Landau and E. M. Lifshitz, *Theory of Elasticity* (Pergamon, Oxford, 1982).

[27] J.D. Eshelby, Solid State Phys. **3**, 79 (1957).

[28] C.L.M.H. Navier, *Résumé des Leçons sur l'Application de la Mécanique* (Dunod, Paris, 1864).

[29] D.S. Chandrasekharaiah and L. Debnath, *Continuum Mechanics* (Academic, San Diego, 1996), p. 218; S. Timoshenko, *History of Strength of Materials* (McGraw-Hill, New York, 1953), p. 229; E.A.H. Love, *A Treatise on the Mathematical Theory of Elasticity* (Dover, New York, 1944); L.E. Malvern, *Introduction to the Mechanics of a Continuous Medium* (Prentice Hall, New Jersey, 1969); I.S. Sokolnikoff, *Mathematical Theory of Elasticity* (McGraw-Hill, New York, 1946).

[30] M. Baus and R. Lovett, Phys. Rev. Lett. **65**, 1781 (1990); **67**, 406 (1991); Phys. Rev. A **44**, 1211 (1991).

[31] In Fourier space, with a unit lattice constant, the derivatives are replaced as $\Delta_{x,y}^2 \to 2 - 2\cos k_{x,y} = 4\sin^2(k_{x,y}/2)$. This Brillouin-zone Fourier substitution is automatically taken care of in simulations by FFT subroutines. To save on notation, we will write in the text $\Delta_{x,y}^2 \to k_{x,y}^2$ with the understanding that the long-wavelength limit $k_{x,y}^2$ actually stands for the sinusoidal lattice

function $4\sin^2(k_{x,y}/2)$. Thus, for example, the discrete Laplacian will be written as $\vec{\Delta}^2 \to \vec{k}^2$ instead of $4-2\cos k_x - 2\cos k_y = 4\sin^2(k_x/2) + 4\sin^2(k_y/2)$. *Functions* like $Q_s(\vec{k})$, $M(k)$ will also use this compact notation ($s=1,2,3$). Of course, *labels* of points in the Brillouin zone $\vec{k}$, still stand for the actual wave vector $\vec{k} = |\vec{k}|\hat{k}$. To emphasize that textural nonuniformity results from the large-scale compatibility properties of the (''anisotropic continuum'') solid, rather than from trivial small-scale discreteness, we use the long wavelength $U(\hat{k})$ in simulations.

[32] G.R. Barsch and J.A. Krumhansl, Metall. Trans. A **19A**, 761 (1988).

[33] For periodic boundary conditions, the strains in a box $L_0 \times L_0$ have the same constant values at opposite box sides: $\varepsilon_\ell(x, y=0, t) = \varepsilon_\ell(x, y=L_0, t)$; $\varepsilon_\ell(x=0, y, t) = \varepsilon_\ell(x=L_0, y, t)$. This is satisfied by expanding in a complete set of plane wave states, as is natural for simulations using FFT routines: $e^{ik_x L_0} = e^{ik_y L_0} = 1$ fixes the wave vector spectrum. The second derivative of strains is consequently periodic. Net dissipation must only occur from Rayleigh terms inside the box, and not over the boundaries. (Ref. 6) The periodic boundary conditions enforce this requirement. The BG equation is also a continuity-type equation, with $\rho_0 \dot{\varepsilon}_\ell(\vec{r},t) \equiv n(\vec{r},t)$ as a ''momentum density'' and $\frac{1}{4}c_\ell^2 \vec{\Delta}\{[\partial(F + F^c)/\partial\varepsilon_\ell + \partial(R+R^c)/\partial\dot{\varepsilon}_\ell]\} \equiv \vec{J}(\vec{r},t)$ as a ''momentum current.'' (Note the $\partial F/\partial\varepsilon_\ell$ term contains a $\Delta^2\varepsilon_\ell$ contribution.) The generalized BG equation is then $\dot{n} = \vec{\Delta}\cdot\vec{J}$. Integrating over the box yields normal components of $\vec{J}$ that add up to zero: the box surfaces have no net frictional losses. (Since periodic boundary conditions are foldings of opposite edges onto each other, there are no real boundaries.) The required condition (Ref. 6) $d(T+V)/dt = -2R$, that energy loss is determined only by the bulk Rayleigh dissipation rate, follows at once, using the strain-acceleration expression (4.4a) of BG dynamics.

[34] For finite systems the no-defect compatibility condition holds, both in the bulk and at the surfaces. Periodic boundary conditions on strains reveal the bulk compatibility potential from internal non-OP strains. The surfaces induce extra non-OP strains that can be shown to produce additional surface compatibility potentials (Ref. 10), which decrease with increasing system size, and can also be written in terms of the bulk OP strains. These will be considered elsewhere, and we focus on periodic boundary conditions, and bulk compatibility, for simplicity.

[35] D.M. Hatch, T. Lookman, A. Saxena, and S.R. Shenoy (unpublished).

[36] The Fourier integral is performed by rotating the wave vector axes by 45°, defining $\tan\gamma \equiv a_1/a_3$ and doing first the k_y and then the k_x contour integrals, and taking the relevant real parts of the residues. Yuri B. Gaididei (private communication).

[37] J.D. Jackson, *Classical Electrodynamics* (Wiley, New York, 1999).

[38] Time delays are also contained in the TR case dynamics, but with mutually nonlinear couplings in both OP strain components there could be a spectrum of mutually driving frequencies.

[39] We use $L_0 \times L_0 = 128^2$ lattices with periodic boundary conditions on the strain (Ref. 33) and Euler routines, with step sizes and parameters as in the figure captions. With notional time units (Appendix B) as picoseconds and number of steps N_t we go up to $t \equiv \Delta t N_t \sim 1000$ ps in some cases. Diagnostics for monitoring textural evolution included the free energy per unit cell $E \equiv F(t)/L_0^2$; forces $\partial F/\partial\varepsilon_\ell(t)$; spatially averaged strains $\langle\varepsilon_\ell(\vec{r},t)\rangle$; and max-min values of $\{\varepsilon_\ell(\vec{r},t)\}, \{e_i(\vec{r},t)\}$. Unless specified, the initial conditions were randomly varying strains with zero spatial average, and amplitudes less than ~ 0.2. For Fourier transforms, if non-OP strains are derived from the OP strains through relations that are ill defined at $\vec{k}=0$, then we set $e_i(\vec{k}=0) = 0$.

[40] A. Saxena, T. Lookman, A. R. Bishop, and S. R. Shenoy, Los Alamos National Laboratory Report No. LA-UR-99-336, 1999 (unpublished).

[41] A. Saxena, T. Lookman, S.R. Shenoy, and A.R. Bishop, Mater. Sci. Forum **327-328**, 385 (2000).

[42] Y.H. Wen, Y.Z. Wang, and L.Q. Chen, Philos. Mag. A **80**, 1967 (2000).

[43] T. Lookman, A. Saxena, S.R. Shenoy, and A.R. Bishop (unpublished).

[44] C. Manolikas and S. Amelinckx, Phys. Status Solidi A **60**, 607 (1980); **61**, 179 (1980).

[45] G.R. Barsch and J.A. Krumhansl, in *Proceedings of ICOMAT-92*, edited by C.M. Wayman and J. Perkins (Monterey Institute of Advanced Studies, CA, 1993), p. 53; M. Sato, B.H. Grier, S.M. Shapiro, and H. Miyajima, J. Phys. F: Met. Phys. **12**, 2117 (1982); T.R. Finlayson, M. Mostoller, W. Reichardt, and H.G. Smith, Solid State Commun. **53**, 461 (1985).

[46] H. Risken, *The Fokker-Planck Equation: Methods of Solution and Applications* (Springer-Verlag, Berlin 1989); H. Haken, *Synergetics: an Introduction* (Springer-Verlag, Berlin, 1983).

[47] V. Balakrishnan, Pramana **11**, 379 (1978); **13**, 547 (1979); *Mechanical Properties of Solids: Plastic Instabilities*, edited by V. Balakrishnan and C.E. Bottani (World Scientific, Singapore, 1986).

[48] H. Goldstein, *Classical Mechanics* (Addison-Wesley, Reading, MA, 1980).

[49] P.C. Hohenberg and B. Halperin, Rev. Mod. Phys. **49**, 435 (1977).

[50] Each of the L_0^2 sites in the Brillouin zone has a two-component oscillator [real and imaginary parts of $\varepsilon(\vec{k},t)$], but since strain is real, the $\vec{k}$ and $-\vec{k}$ oscillators are images of each other (with real part the same, imaginary part π out of phase). Thus there are L_0^2 independent degrees of freedom.

[51] For zero initial macroscopic strain rates and strains, quasiconservation is observed: the final diagnostics are $\langle\varepsilon_\ell\rangle \sim 10^{-3}$, with max-min ε_ℓ of order unity, (varying by a few tenths of a percent over time near the end of a run).

[52] In Fourier space the effective elastic constant $A(k) \equiv F_0'' + a_1 U^c + K_0 k^2$ in the Fourier version of Eq. (5.5) makes larger k strains relax faster, giving a weaker form of sequential-scale BG relaxation. Indeed when $K_0 = 0$, we get blobs instead of well-defined textures.

[53] T. Lookman, S.R. Shenoy, K. Ø. Rasmussen, A. Saxena, and A.R. Bishop, in *Proceedings of ICOMAT'02*, 2002 (unpublished).

[54] Taking the top right panel of Fig. 8 of energy per unit cell $E_0 = -1.468$ as a reference, the fractional differences $\delta = (E - E_0)/E_0$ of the two quasitwin pictures are $\delta = 0.0391$ and 0.0392. For yet another random-number seed a uniform state results, with no domain walls (not shown).

[55] J. Schmalian and P.G. Wolynes, Phys. Rev. Lett. **85**, 836 (2000).

[56] L.D. Landau and E.M. Lifshitz, *Statistical Physics* (Pergamon Press, Oxford, 1980); L.D. Landau, Phys. Z. Sowjetunion **8**, 113 (1935); **11**, 26 (1937).

[57] W. Klein, T. Lookman, A. Saxena, and D.M. Hatch, Phys. Rev. Lett. **88**, 085701 (2002).

[58] Symmetry allowed couplings between strain and another functionality, which typically has nonlinear terms, lead to a long-range interaction in the second moment of the functionality. For example, for 2D SR ferroelectrics the coupling terms in the free energy are of the form $R\varepsilon$, Se_1, Te_2, where $R=P_x^2-P_y^2$, $S=P_x^2+P_y^2$, $T=P_xP_y$ and P_x,P_y are components of the polarization vector $\vec{P}$. Eliminating the elastic strains [elastic energy $F_e=(A_\varepsilon/2)\varepsilon^2+(A_1/2)e_1^2+(A_2/2)e_2^2$] leads to an effective contribution to the free energy in P_x,P_y of the form $\int [R(r)G(r-r')R(r')+S(r)G(r-r')S(r')+T(r)G(r-r')T(r')]\,dr\,dr'$, where $G(r)\sim 1/r^2$.

[59] The scaled geometric nonlinearity contributions are relatively negligible for $ka_c\lambda \ll 1$ at long wavelengths, were a_0 is the unit-cell scale and λ is a characteristic strain. A sufficient condition for using the form (2.2) is $\lambda \ll 1$. In the kinetic energy, the total time derivative (Ref. 29) $D\vec{u}/Dt=\partial\vec{u}/\partial t+\lambda(\vec{u}\cdot\vec{\Delta})\vec{u}$ in general contains ''convective terms'' that are relatively negligible in the same regime $ka_0\lambda \ll 1$. Thus for $\lambda \ll 1$ convective terms are ignored for consistency.